

An overview of flow cell architectures design and optimization for electrochemical CO₂ reduction

Dui Ma,^{ac} Ting Jin,^{*ab} Keyu Xie^{*ab} and Haitao Huang^{*c}

^a Research & Development Institute of Northwestern Polytechnical University in Shenzhen, P. R. China. E-mail: kyxie@nwpu.edu.cn

^b State Key Laboratory of Solidification Processing, Center for Nano Energy Materials, School of Materials Science and Engineering, Northwestern Polytechnical University and Shaanxi Joint Laboratory of Graphene (NPU), Xi'an, 710072, P. R. China. E-mail: tjin@nwpu.edu.cn

^c Department of Applied Physics and Research Institute for Smart Energy, The Hong Kong Polytechnic University, Hung Hom, Kowloon, Hong Kong, P. R. China. E-mail: aphhuang@polyu.edu.hk

Keywords: CO₂ electroreduction, flow cell electrolyzers, reactor architectures, system engineering, parametric optimization

Converting CO₂ into value-added fuels or chemical feedstocks through electrochemical reduction is one of the several promising avenues to reduce atmospheric carbon dioxide levels and alleviate global warming. This approach has mild operating conditions, adjusts product distribution, allows modular design, and offers opportunities for carbon-intensive manufacturing industries to utilize renewable energy power for CO₂ reduction. In recent decades, various valid methods and strategies have been developed for high efficiency and high selectivity electrocatalysts to reduce CO₂. Unfortunately, while intensive research focuses on the development of new electrocatalysts, little attention has been received in the engineering design of low-cost and large-scale CO₂ reduction electrolyzer architectures, which impairs the full realization of potential benefits of new electrocatalysts. This review summarizes the recent progresses of the reactor architectures and system engineering in CO₂ reduction reaction. We discuss how to improve the performance of CO₂ reduction reaction from four aspects: (i) flow cell architectures, (ii) management of reactant delivery, (iii) membranes, (iv) electrolytes. We

aim to introduce the reactor architectures and system engineering strategies in detail to provide further development and inspiration for potential industrial applications of CO₂ reduction.

1. Introduction

Energy available from burning fossil fuels has, thus far, been the main means to solve our ever-growing global energy demands. However, from the perspective of sustainable development, the massive CO₂ emission from the misuse of fossil fuels brings about the “greenhouse effect”, which has led to severe consequences on our environment in the form of global warming, climate changes, the disruption of carbon cycle in nature, and even extinction of species, etc.¹⁻

³ To protect our environment for a sustainable future, it is imperative to urgently decrease atmospheric CO₂ levels to an appropriate level for minimizing damage to the environment. Since fossil fuels are non-renewable energy sources, continued and unchecked use will eventually lead to their depletion. Clean energy sources like solar energy, wind energy, and hydropower, which produce little or no carbon footprint, tackle the parallel challenges mentioned above.⁴ However, many challenges need to be addressed before these energy carriers, such as H₂, methanol, ethanol, and methane, are widely used.

If CO₂ becomes a renewable raw material for fuels, commodities, medicines, and laboratory chemicals that we need to maintain our society, then we can achieve an economy circle based on renewable energy and carbon dioxide. This solves both the energy crisis and the environmental issues, killing two birds with one stone. To date, a number of carbon capture, storage, and utilization strategies have been proposed to reduce anthropogenic CO₂ emissions from the exhaust gases generated during heavy industrial manufacturing processes.⁵⁻¹³ In recent

years, electrochemical CO₂ reduction reaction (CO₂RR) has become a more attractive strategy due to its intriguing merits (Fig. 1). Intermittent renewable energy can be used as electricity to reduce CO₂ into a variety of fuels or valuable chemical products, including CO, formic acid, acetate, hydrocarbons, and alcohols, with net-zero CO₂ emissions and simultaneous environmental remediation of CO₂ greenhouse gas. It solves the electricity supply and demand mismatch problem caused by geographical location and seasonality. Meanwhile, the reaction process can be environmentally friendly and pollution-free production. Besides, electrochemical cells operate under mild conditions, generally at normal pressure and temperature, and the whole process and direction are controlled by the reduction potential. What's more, electrochemical systems require relatively simple and small workshops, and can use modular design and scalable equipment. The electrocatalytic systems are expected to be incorporated with gas diffusion electrodes (GDEs) and flow reactor configurations for industrial production.

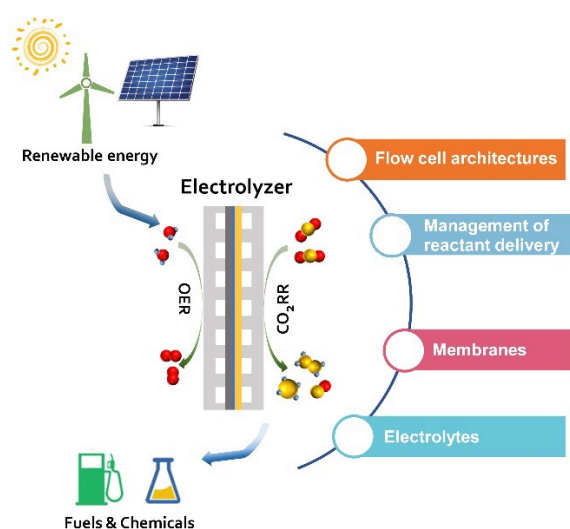


Fig. 1 A schematic diagram of electrochemical CO₂ reduction by system engineering.

The structure design of electrocatalytic reactors is a far-reaching subject, which affects the key factors during the CO₂RR, such as current density, Faradaic efficiency (FE), selectivity,

catalytic stability, and product separation, etc. Until now, the typical H-type electrolytic cell remains the most common lab-scale reactor for CO₂RR, on account of its facile assembly, easy operation, and low cost.¹⁴ As illustrated in Fig. 2a, the reactor is separated into independent cathode and anode compartments by an ion-exchange membrane. The reference and the working electrodes are located in a sealed cathodic chamber, while the counter electrode is placed in the anodic chamber, forming a three-electrode system. The low CO₂ solubility in aqueous solution limits its mass transport, making the CO₂ reduction current densities below 100 mA cm⁻².¹⁵⁻¹⁷ In addition, other inherent defects, including limited electrode surface area and far interelectrode distance, can no longer meet the increasing research and potential industrial application requirements. Thus, the H-type cell configurations are difficult to commercialize for large-scale implementation.¹⁸

To improve the CO₂ conversion rate to a meaningful level, electrochemical CO₂RR must be carried out using a continuous flow equipment to conquer the limitation of mass transport. The thermodynamics and kinetics of the CO₂RR in flow reactors are fundamentally different from those in an H-type cell, due to a higher CO₂ concentration on the electrocatalyst surface, a shorter transmission path, and a suitable gas diffusion layer substrate.

At present, the CO₂RR flow electrolyzers are still not mature in industry, but recent research works have shown the prospect of industrialization. In this review, we will sum up the currently known types of flow reactors and their components, targeting on the general strategies for improving the core performance indicators of catalytic current density, selectivity, and energy conversion efficiency. We will focus on the influence and optimization of each component in flow cell systems, so that researchers can have a clearer understanding of the choice of flow

reactors. We also hope to provide meaningful, timely, and valuable guidance to the design and commercialization of advanced flow electrolyzers for CO₂ reduction in the near future.

2. Flow cell architectures

2.1. Membrane-based flow cell

Over the last decades, membrane-based flow cells evolved from fuel cells or water electrolyzers have received extensive attention owing to their effective mass transfer efficiency and large current density (more than 100 mA cm⁻²). Fig. 2b depicts the typical structure of a membrane-based flow cell, in which a polymer electrolyte membrane (PEM) serves as a separator sandwiched between the flowing anode and cathode electrolytes to facilitate the ion flow and attenuate product crossover.¹⁹ Both a CO₂-saturated cathode electrolyte and an anode electrolyte can be continuously circulated through the pump, while the gaseous CO₂ as the reactant is directly transported to the reverse side of the gas diffusion electrode covered by the cathodic catalyst. Compared with conventional H-type cells, the thermodynamic and kinetic characteristics of the CO₂RR in flow reactors vary greatly because of the higher CO₂ concentration on the electrode surface, direct contact effect between the polymer membrane and the catalyst surface, and the available range of electrocatalyst substrates. Therefore, flow reactors have better efficiencies in electrochemical CO₂ reduction and is a more appropriate technology for large-scale commercial applications.²⁰⁻²²

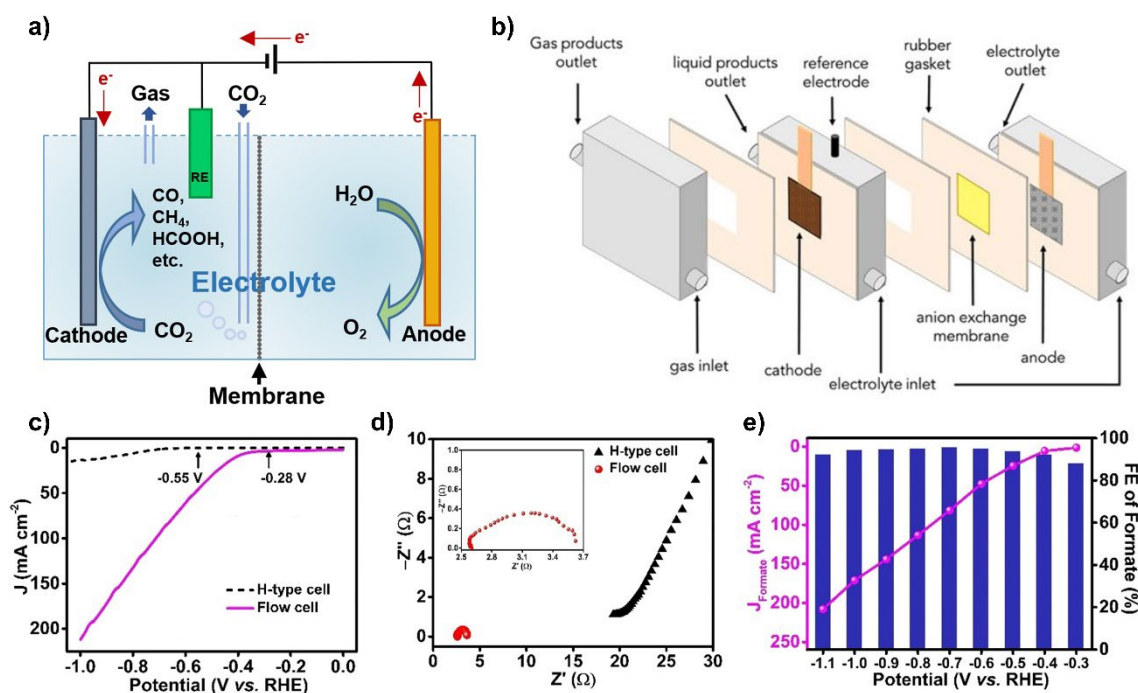


Fig. 2 (a) Schematic illustration of H-type cell. (b) A membrane-based flow cell for CO₂ reduction. Reproduced with permission.¹⁹ Copyright 2020, Elsevier. (c) LSV curves and (d) Nyquist plots of Bi₂O₃@C-800 based on H-type cell and flow cell. (e) FE and partial current density of formate for Bi₂O₃@C-800 in a flow cell. Reproduced with permission.²³ Copyright 2020, Wiley-VCH.

Recently, Xia et al. found that the onset potential of Bi₂O₃@C-800 catalyst based on the membrane-based flow cell was as low as -0.28 V vs. RHE, the formate FE was consistently above 93% in a very wide potential window between -0.3 V to -1.1 V vs. RHE, and the partial current density of formate can reach 208 mA cm⁻².²³ However, the onset potential and the partial current density of formate in the H-type cell were -0.55 V vs. RHE and ~ 12 mA cm⁻², respectively (Fig. 2c-2e). The results revealed that the Bi₂O₃@C-800 catalyst can achieve high selectivity and high current density for formate production in the flow cell, which is ascribed to the decreasing ohmic resistance and the high concentration KOH electrolyte based on the flow cell configuration. Similar to the above conclusion, Cao et al. reported that the as-obtained atomically thin bismuthene coupled with a high activity (the ultrahigh current densities ~300

mA cm⁻²) and selectivity (Faradaic efficiency nearly 100%) for formate over a record wide potential range from -0.83 to -1.18 V vs. RHE in a flow cell.²¹ The remarkable performance improvement of the flow cell can be attributed to the mass transfer characteristics of GDE, reduced the reaction overpotential, and suppressed the competing HER.

Generally speaking, similar to fuel cells, membrane-based flow cells are one of the most promising candidates for large-scale commercial applications due to their compact structures and high current densities. However, there are still many factors restricting their development. Further study on the influence of different factors such as reactant phases, electrode substrate, polymer electrolyte membranes, and catalysts, must be conducted, and the excessively high overpotential is also a big challenge.

2.2 Microfluidic flow cell

Kenis and his co-workers pioneered and developed a microfluidic flow cell for electrochemical CO₂ reduction.²⁴⁻²⁷ As depicted in Fig. 3a, two gas diffusion electrodes are coated with a cathode catalyst for CO₂ reduction and an anode catalyst for oxygen evolution reaction, respectively.²⁵ The continuous flow of CO₂ as a reactant directly inputs and rapidly diffuses to the catalyst and electrolyte interface *via* a gas diffusion layer (GDL). Additionally, this structure relies on an ultrathin flowing electrolyte channel (< 1 mm thickness) to separate the anode and cathode. Unlike membrane-based flow cells, under laminar flow conditions with this microfluidic flow configuration, the intersection of reactants and products is controllable due to the slow diffusion of products. Thus, microfluidic electrolytic reactors not only avoid the use of costly membranes, but also allow flexible management of operating conditions, including the electrolyte composition and pH. Also, they alleviate the anode drying and cathode flooding

that are caused by the permeability resistances of water molecules and the proton transport through the membrane, respectively, when operating at high current densities.

Xuan and his colleagues developed and validated a numerical model for CO₂ utilization and fuel production processes based on the microfluidic system.²⁸ By analyzing the mass transfer and electrochemical performance of the cathode side of the microfluidic system, they pointed out that the low diffusion rate of CO₂ in GDE, competitive HER, and the hydrogen dilution effect are the key factors limiting the performance of electrodes and resulting in low efficiency. HER kinetics and CO₂ feed rate can be further optimized to improve the performance. In particular, they systematically studied the benefits of CO₂ utilization in a dual electrolyte microfluidic reactor (DEMUR) system through a series of experiments and theoretical models.²⁹⁻

³² As shown in Fig. 3b, due to the inflow of two different electrolytes, a virtual separation interface dominated by acid-base interfacial heat is formed between the cathode and the anode. The ohmic Joule heat is much smaller than that of a single electrolyte system, thereby improving the electrochemical performance. They concluded that a pH 2 cathode electrolyte and a pH 14 anode electrolyte output the best formic acid production cell performance, which was also verified by model calculations. In addition, they also pointed out that identifying optimized microfluidic design dimensions and electrolyte recycling in a microfluidic pH-differential network would be feasible under proper adjustment of operating conditions. Moreover, **Raman et al. used a mechanistic mathematical model to conduct a Monte Carlo simulation of CO₂ to CO conversion in a microfluidic flow cell reactor.**³³ They have investigated the effects of a variety of parameters (geometric/design, physical, material, operating, and electrochemical parameters) on the performance, conversion efficiency, and selectivity of the microfluidic

system. They proposed simplified regression models through supervised machine learning algorithms to forecast the overall performance of devices without solving the complete system. The results showed that the properties of the catalyst characterized by the charge transfer coefficient are the most significant parameters affecting the cell performance in the overall cell potential range. In addition, even if the random input parameters are normally distributed, the reactor output performance is not a normal distribution under the entire cell potentials, indicating that it is necessary to combine practical experiments to obtain the optimal reactor performance. In short, both experimental and numerical model research on the effects of microfluidic flow cells provides a new opportunity for fundamental studies about the CO₂ reduction process, thereby providing new perspectives for technological improvement.

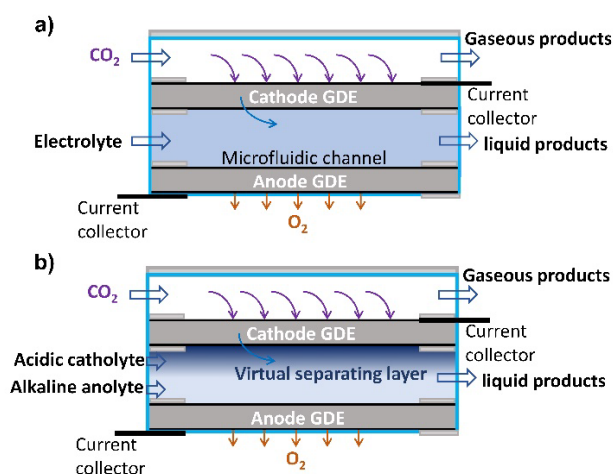


Fig. 3 Schematic diagrams of (a) the microfluidic reactor and (b) a dual electrolyte microfluidic reactor for CO₂ conversion.

2.3 A cell with gapless electrode

A cell with gapless electrode is an emerging type of electrolyzer, which presses the cathode and anode electrodes together with an ion-exchange membrane in the middle to create a zero-gap cell (Fig. 4a). The continuously humidified CO₂ stream is directly supplied to the cathode. CO₂ reduction occurs at the boundary between the membrane and the cathode electrode. The main

advantage of this device over a microfluidic flow cell is that it is relatively easy to significantly increase the local CO₂ concentration by pressurizing and thus produces higher current density and reaction rate.³⁴⁻³⁸ In addition, cells with gapless electrodes have a distinct advantage over membrane-based flow cells in that they have a lower ohmic loss and reduce the risk of catalyst poisoning caused by impurities in the cathode electrolyte. However, a potential drawback of zero-gap cells is that liquid products from CO₂ reduction (such as alcohols) may backflow into GDE pores and choke the catalytic active sites, thus impeding the entry of CO₂ reactants. This means that the liquid products may penetrate the gas flow channel to prevent further reaction, which has a great relationship with the GDEs. We provide further discussion of GDEs in Section 3.3.

Most cells with gapless electrode reported in the literature use a cation exchange membrane to transport protons for CO₂ reduction.¹⁶ Park and co-workers proposed a gaseous CO₂ supply to improve the electrolytic performances of the CO₂ reduction with circumvention of the CO₂ solubility limitation.³⁹ They revealed that the formate formation was more stable in a CO₂-fed electrolyzer than in a liquid electrolyte-supplied electrolyzer, which was benefited from shortened CO₂ diffusion pathway to the tin nanoparticle catalyst. However, the accelerated ion exchange rate facilitates the acidification of the catholyte and promotes the competitive hydrogen evolution reaction (HER).⁴⁰⁻⁴¹ To address this problem, Neyerlin and co-workers inserted a thin catholyte layer between the cathode and membrane to maintain the proper pH near the cathode for CO₂ reduction reaction (Fig. 4b-4c).⁴² In an alternative design, Mallouk and co-workers displayed a vapor-fed electrolyzer with a bipolar membrane that can achieve a more stable cell voltage than an electrolyzer with a cation exchange membrane during a 12 h

CO₂ reduction process on account of the better control of pH by the bipolar membrane.³⁵ Recently, Sargent et al. operated the anion exchange membrane cell with gapless electrode based on the Cu surface coated with a nitrogen-doped carbon layer catalyst, and delivered ethanol FE of 52%, achieving the cathodic energy efficiency (EE) of 31% and full-cell EE of 16% for ethanol.³⁶ Moreover, considering the similarity between these devices and PEM fuel cells, it seems more straightforward to scale them up to an industrial scale and build large sized stacks.

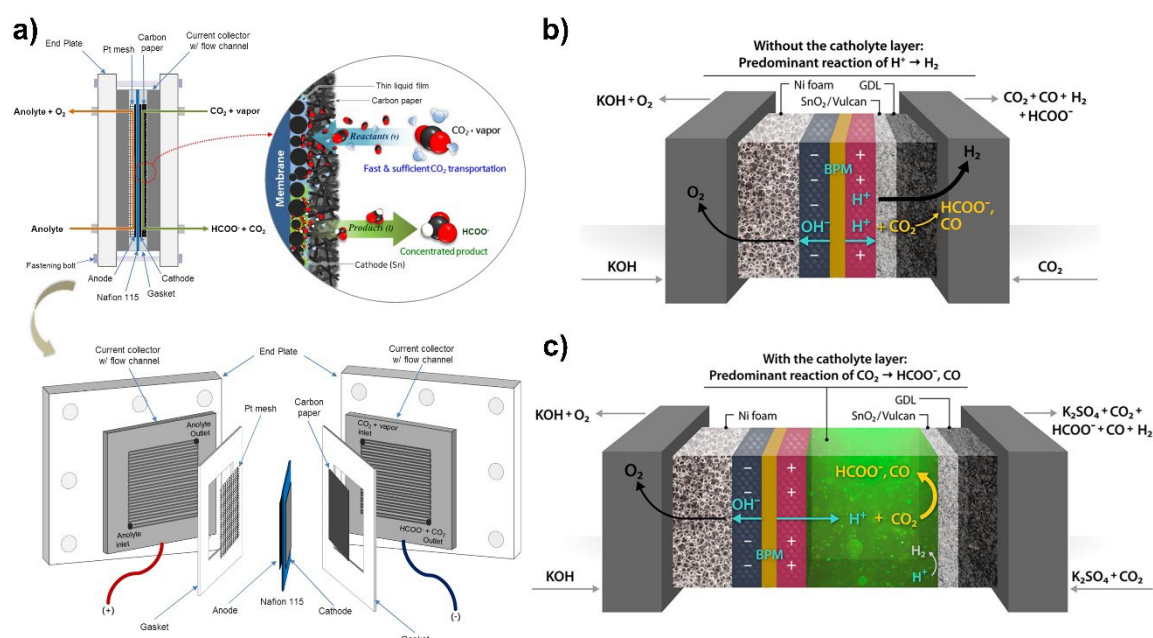


Fig. 4 (a) Construction of a cell with gapless electrode for CO₂ electroreduction. Reproduced with permission.³⁹ Copyright 2018, Wiley-VCH. Schematic illustrations for (b) a full BPM zero-gap cell setup and (c) a novel cell with a thin layer of catholyte buffer. Reproduced with permission.⁴² Copyright 2020, American Chemical Society.

3. Management of reactant delivery

3.1 Flow field design

The delivery and/or management of water and CO₂ is affected by the mild chemical cell macro geometry components, which control the hydrodynamics of the gas/liquid flow in the cell.

Bipolar plates with flow fields can influence the distribution of CO₂ and/or H₂O across the flow

electrolyzers by adjusting the flow field factors such as channel width, rib width, depth, and the ratio of channel width over landing width. A critical challenge for flow field design is how to improve the fluid management via a suitable flow field pattern. Most literature reports are based on computational fluid dynamics simulation, water gradient mapping, and tests on pressure/temperature sensing under different flow fields to better understand the effects of these geometric parameters on electrolysis performance.⁴³⁻⁴⁴ The effects of flow field architectures on PEM fuel cells⁴⁵⁻⁴⁷ and redox flow batteries⁴⁸⁻⁴⁹ have been extensively studied, but they are far from a precise understanding in the environment of CO₂ reduction. The flow field architecture techniques, which have been applied to commercial fuel cells and redox flow batteries, however, provide a blueprint for CO₂ electroreduction.

Typical flow field designs are the parallel flow field (PFF), serpentine flow field (SFF), and interdigitated flow field (IFF) (Fig. 5a-5c). The original design of the parallel flow channel is to reduce pressure drops and improve efficiency. However, in this kind of PFF, water tends to accumulate from small droplets to large droplets and block the flow channel. In addition, poor design could also cause inhomogeneous reactant gas-distribution or even bypass parts of the active area, which may also affect the performance of the device due to insufficient reaction gas on the electrode.

SFF is the most common flow channel trend and has also been most widely studied.⁵⁰⁻⁵¹ As shown in Fig. 5b, there is only one flow path from the inlet to the outlet on the entire plate. It can rapidly drain the cell products without the liquid blocking the runner that occurs in some other flow channels. However, for a large-area plate, the flow channel is too long, resulting in a large pressure drop between the inlet and the outlet and uneven current density distribution.

These lead to large parasitic energy requirements. Especially in the case of small portable flow cell systems, the energy required to transport the fluids should be as small as possible.

As illustrated in Fig. 5c, the IFF can highly improve the cell power density. Its characteristic is that the fluid is mandatory to pass through the diffusion layer, while other forms of flow channels penetrate the diffusion layer mainly under their pressure. The significant advantage of the IFF is that the fluid can fully pass through the diffusion layer. However, due to the large resistance of the diffusion layer and the large pressure drop of the fluid, the catalytic layer of the reactor may be destroyed, leading to poor equipment performance. Besides, the interdigital flow channel is more prone to short-circuit in the case of poor design, resulting in a decrease in the utilization rate of reactants and electrodes. In addition to the above-mentioned common flow fields, several new types of field designs such as spiral flow field⁴⁵, fractal flow field⁵², tubular flow field⁵³, circular flow field⁴⁴ and corrugated flow field⁵⁴ have also been proposed to improve the uniformity of flow distribution and enhance the localized mass transfer in the porous electrode.

Ibrahimoglu et al. showed that the velocity and pressure distributions of the gases in the spiral flow field are uniform using the computational fluid dynamics method, which can reduce the pressure drop per unit length of the flow field, but it has considerable ohmic losses and higher efficiency in auxiliary power consumption.⁴⁶ Berlinguette and co-workers reported the use of 3D printing technology to electroplate nickel on plastic flow slots, which enables rapid prototyping and optimization of experimental flow plates with different geometric shapes for water electrolyzers.⁵⁵ Recently, mixed-flow field designs (e.g., multiple serpentine, segmented serpentine, and straight and parallel flow fields) have been applied to study the influence on

degradation behavior associated with potential cycling (Fig. 5d-5f).⁵⁶⁻⁵⁷ These studies also emphasized the importance of proper flow field design for long-term operation under adverse conditions.

In brief, different flow field designs have both pros and cons. Therefore, in the employed device, the distribution of reactants flow field must always be optimized to achieve targeted applications, thereby minimizing nonuniformity, reducing the dead zones and improving the utilization rate of reactants. The use of bipolar plates with flow patterns requires extensive research in flow electrolyzers, and the use of different flow fields may help scale up and industrialize this process.

3.2 Gas-phase CO₂ fed

Generally speaking, in a typical CO₂ reduction electrolytic reactor, CO₂ can be transported to the cathode in two forms: dissolved in a mild alkaline solution (usually an aqueous bicarbonate solution) or directly in a gas-phase. However, because of the inherent low diffusion and low solubility of CO₂ in aqueous media, the current density of CO₂ reduction in the bulk liquid phase is limited to around 30 mA cm⁻², representing a significant mismatch between in-service catalytic oxygen evolution and catalytic CO₂ reduction.¹⁹ Although the continuous flow of electrolytes can conquer the limitation of CO₂ diffusion in the liquid phase to some extent, the CO₂ concentration in aqueous solution is essentially limited by environmental conditions. Alternatively, pure CO₂ gas can be directly sent to the cathode to increase the concentration of effective CO₂ molecules on the surface of the cathode catalyst, thereby improving the reaction rate.

The earliest example of a standard PEM electrolyzer modified by directly feeding gaseous CO₂ to cathode can be traced back to 1995. At that time, Nishimura et al. reported that the current efficiency was increased to 90% for CO production on Au electrode through the improved device.⁵⁸ After decades of research, feeding gaseous CO₂ to the cathode with CO₂-saturated aqueous electrolyte became popular to be assembled into a membrane-based flow cell to form a variety of products, such as CO⁵⁹, formate⁶⁰, alcohols⁶¹, and hydrocarbons⁶². Lately, fluorine-modified Cu-based gas diffusion electrodes exhibited a C₂₊ (mainly ethylene and ethanol) formation rate of over 4.0 mmol h⁻¹ cm⁻² with an ultra-high current density of 1.6 A cm⁻² and a selectivity of 80% Faradaic efficiency based on a flow cell fed directly by CO₂, which is significantly superior to those reported up to now.⁶³ In fact, a growing number of recently reported examples tend to combine CO₂ gas reactants with gas diffusion electrodes that validate its effectiveness in achieving high reaction rates and efficiencies.

In order to convert a large amount of CO₂, how does the flow rate of the gaseous supply affect the current density and FE of the conversion process? It is necessary to note that although the gas flow unit can be employed to describe the overall flow of gas well, it only provides the actual flow of CO₂ reaching the electrolytic cell by the gas flow controller. Consequently, it is very difficult to study and compare electrolyzers with different sizes in different laboratories. Standardizing the gas flow rate by using the free volume of the cathodic chamber of the electrolytic cell and/or the electrochemical active surface area of the electrode seems to be a feasible approach in order to obtain the actual flow rate of CO₂ gas. Surprisingly, there is currently no explicit definition of what the flow rate of CO₂ in an electrolytic cell means.

Recently, some studies on the influence of CO₂ flow rate on the performance of CO₂RR have been reported successively.^{32, 64} They demonstrated that when the reactant CO₂ feed rate is lower than a certain level, the dynamic limitation is not dominant and the effect of gas rate is not noticeable. As the CO₂ flow rate increases, the enhancement of FE is consistent with the simultaneous increase of current density. When the flow rate reaches a certain threshold, the stable behavior achieved shows that most of the catalytic active sites participate in the reaction and reach a state controlled by kinetics (Fig. 5g-5h). In addition to the achievable current density and FE, the flow rate can also adjust the product distribution of CO₂RR. McIlwain and co-workers showed that the H₂:CO ratio in product syngas can be tailored between 1:4 and 9:1 by regulating the current density and the flow rate of CO₂ gas (Fig. 5i).⁶⁵ Unsurprisingly, increasing the concentration of CO₂ on the electrode surface can increase the ratio of the mixed gas CO:H₂. The proportion of product could maintain for 4 hours after a short induction period. The above data suggest that the optimization of the flow rate greatly affects the CO₂RR performance, including the current density, FE, and product distribution.

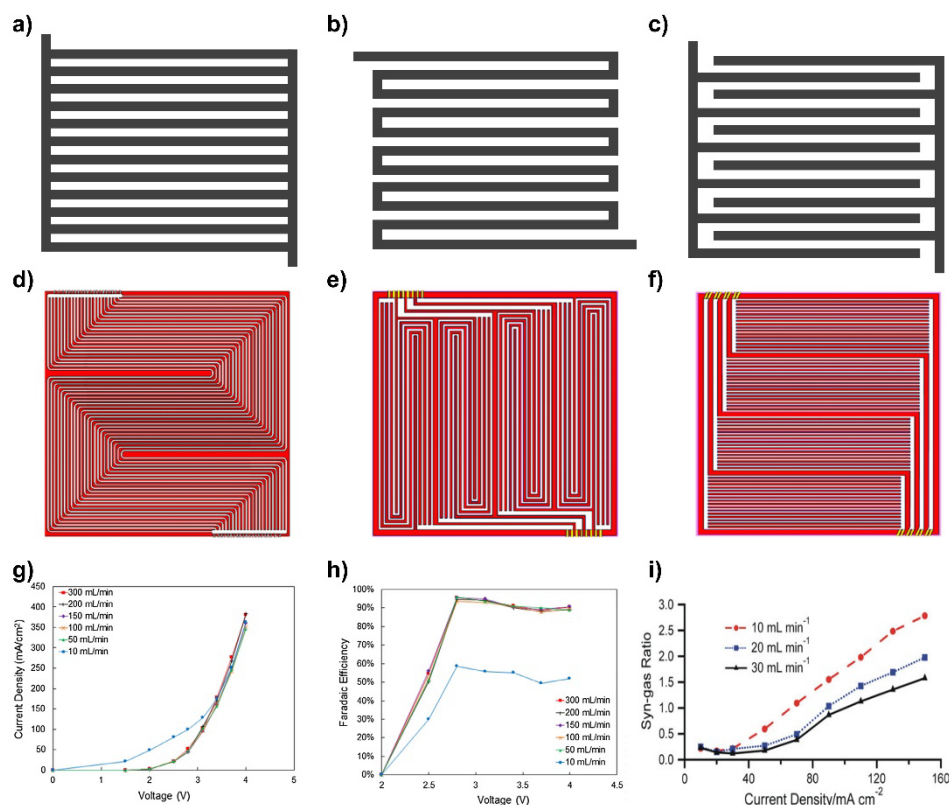


Fig. 5 (a) PFF. (b) SFF. (c) IFF. Flow field designs investigated (d) multiple serpentine, (e) segmented serpentine and (f) straight and parallel. Reproduced with permission.⁵⁶ Copyright 2019, Wiley-VCH. (g) Polarization curves and (h) FEs at different gas flow rates of CO₂. Reproduced with permission.³² Copyright 2017, Elsevier. (i) Syngas (H₂:CO) ratio as a function of CO₂ flow rate. Reproduced with permission.⁶⁵ Copyright 2011, Springer Netherlands.

3.3 Gas Diffusion Layer

Gas diffusion electrodes (GDEs), which create an effective three-phase interface for gaseous reactants, electrodes, and electrolytes, provide a promising avenue to boost the mass transfer process and overall CO₂RR rates. As early as 1990, Sammells et al. published the first report on the use of GDEs to reduce CO₂.⁶⁶ Subsequently, more and more researches on GDEs for CO₂ reduction have been developed and reported.⁶⁷⁻⁷⁰ Fig. 6a shows the typical GDE architecture, where the gas diffusion layer (GDL) can quickly transfer gaseous CO₂ to the catalyst layer (CL). The GDL is usually a porous matrix consisting of densely packed carbon fibers and more tightly arranged microporous carbon layers. More generally, the carbon fibers

can be carbon paper or carbon cloth, and the microporous carbon layers can be carbon nanofibers or compressed carbon powder. The GDL could offer abundant gaseous CO₂ with a much shorter diffusion pathway. At the same time, because of its low resistance, the GDL can also be used as a transport medium for protons, electrons, and products to enter the electrolytic liquid phase from the CL surface. Notable results have been achieved in prolonging the contact time between the reactant and catalytic sites to improve the mass transfer efficiency and current density for electrochemical reactions by the combined properties of the GDEs.

A key characteristic of the GDL is that it must be hydrophobic, otherwise, the liquid electrolyte will penetrate the gas flow channel to block the further reaction. In other words, the GDL must be air-wet, not moistened by the electrolyte. It should be emphasized that the GDL requires suitable hydrophobic properties. Excessive hydrophobicity will result in inferior electronic conduction owing to a large quantity of non-conductive hydrophobe, while insufficient hydrophobicity will restrict the diffusion of gas CO₂ because of the tendency of flooding and accelerate undesired HER (Fig. 6b).^{50, 71} Besides, during the electrochemical reaction process, the GDL surface may change from hydrophobicity to hydrophilicity due to oxidation reaction that occurs at elevated overpotentials and/or applied current density, resulting in flooding of GDL and thereby obstructing the diffusion pathway of CO₂.

In a recent publication, Brushett et al. investigated Ag-coated GDE flooding in a flowing electrolyte and gas-fed CO₂ reduction electrolyzer.⁵⁰ They showed that the molar fraction of CO in the product gas using the Ag-coated GDEs for more than 5 hours was near 95%, while the peak CO performance could only be maintained for less than 15 minutes at 196 mA cm⁻². This means that the faradaic current accelerates the electrode flooding and failure (Fig. 6c). The

authors also proposed that proper microstructures and wettability of GDEs can accelerate the removal of carbonate from the gas liquid interface, thereby alleviating precipitation/flooding events and promoting the long-term high CO₂ conversion rates. It is noted that Zhang et al. recently used a typical Au/C gas diffusion electrode as the model to investigate wettability of gas-liquid-solid three-phase interfaces during CO₂ electroreduction (Fig. 6d-6h).⁷¹ In addition to the use of water droplet contact angle method to evaluate the hydrophilic and hydrophobic properties of different electrodes, they used confocal laser scanning microscopy to intuitively watch the structure of gas-liquid-solid three-phase interfaces, showing that the depth of electrolyte penetration was increased with the increase of hydrophilicity of the electrode surface. They further proved that the transport of CO₂ at the interface plays an essential role in defining the stability of CO₂ equilibrium concentration during CO₂RR.

Furthermore, the stability of GDEs is also a vital problem to be considered and solved, because the long-term stable operation is the key to the realization of the practical application of flow reactors. Although the flow cell system equipped with GDE has achieved excellent CO₂ reduction performance, due to the weak mechanical adhesion between CLs, GDLs, and binder layers, their stability is still poor and needs further development.⁷² With this in mind, Sargent and co-workers developed a viable strategy by integrating polytetrafluoroethylene (PTFE) hydrophobic scaffolds into GDEs, thus constructing a stable and excellent sandwich-like electrode, as shown in Fig. 6i. As a result, the graphite/carbon NPs/Cu/PTFE electrode reduced CO₂ to ethylene with 70% FE at -0.55 V vs. RHE in 7 M KOH solution and can be operated for 150 hours, which was 300 times longer than the traditional GDEs (Fig. 6j).⁷³ The improvement of long-term stability was mainly due to the significantly enhanced hydrophobicity and flood

resistance of the modified GDEs. **Hydrophobic polymers or ionomers integrated into GDEs may have an impact on the electrode performance.**⁷⁴⁻⁷⁶ In general, GDL is an important component of the electrolyzer, and it is necessary to further study the integration with the catalyst layer to improve the CO₂ reduction performance.

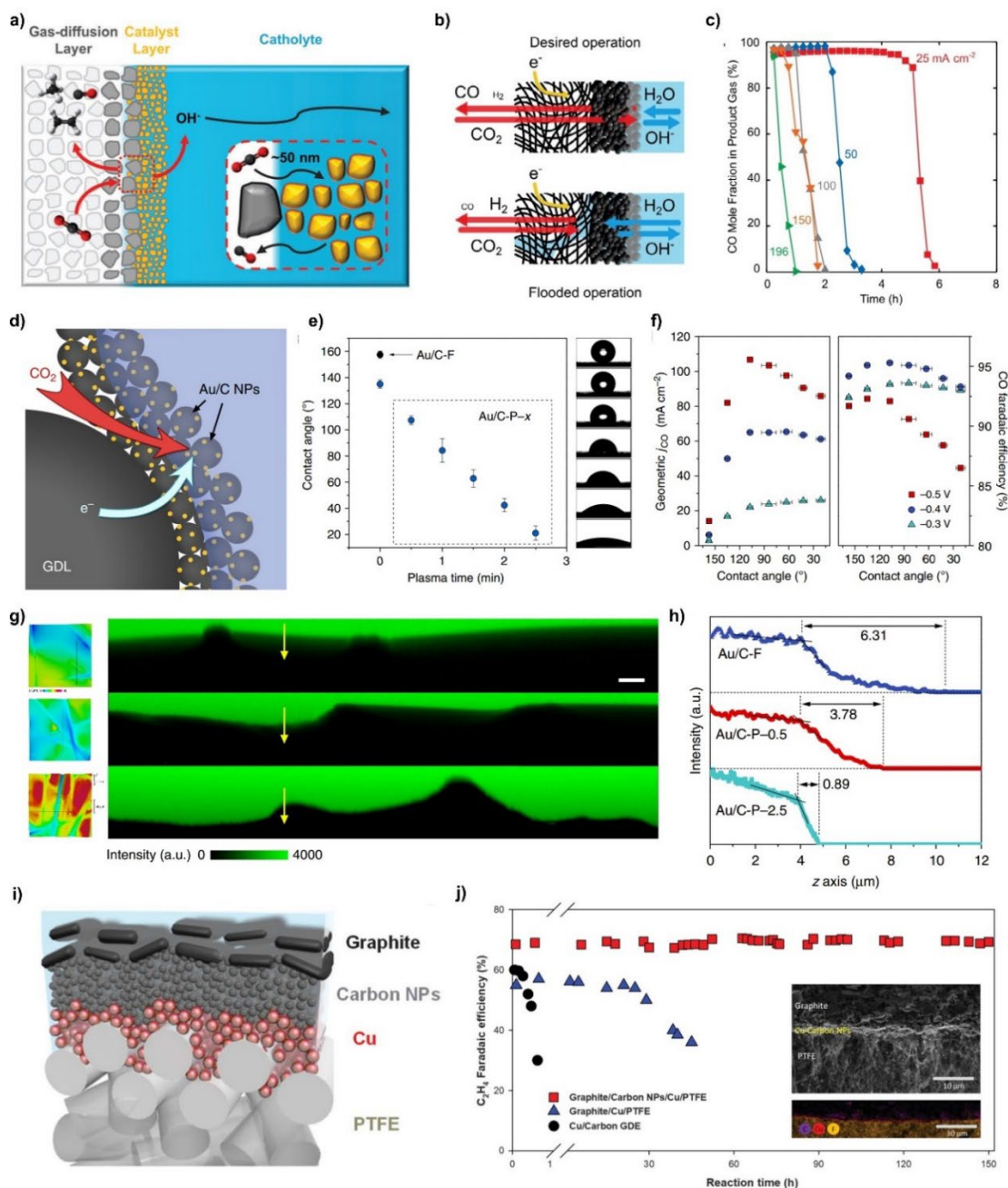


Fig. 6 (a) A catalyst layer deposited onto a hydrophobic substrate. Reproduced with permission.⁷² Copyright 2019, Royal Society of Chemistry. (b) Desired and flooded operations. (c) The mole fraction of CO versus time. Reproduced with permission.⁵⁰ Copyright 2020, Wiley-VCH. (d) Schematic illustration of the gas-liquid-solid three-phase interfaces. (e)

Diagrams and photographs of average water droplet contact angles on different Au/C electrodes. (f) Geometric j_{CO} and FE_{CO} . (g) Cross-sectional fluorescence images scanned according to black lines. (h) Corresponding z axis fluorescence intensity line scans of yellow arrows regions in (g). Reproduced with permission.⁷¹ Copyright 2020, Springer Nature. (i) Schematic illustration of the graphite/carbon NPs/Cu/PTFE electrode. (j) Long-term performance test of CO₂RR. Reproduced with permission.⁷³ Copyright 2018, American Association for the Advancement of Science.

4. Membranes

The polymer electrolyte membranes (PEMs) separate the cathode and anode of the electrolytic device and regulate the flow of half-reacted ions to the other compartment while diminishing product crossover. They also provide mechanical support to withstand pressure differences between the compartments. Three classes of membranes have been employed for CO₂ reduction systems, including cation (or proton) exchange membranes (CEMs)⁷⁷, anion exchange membranes (AEMs)^{62, 78} and bipolar membranes (BPMs)⁷⁹⁻⁸⁰, similar to those in water splitting electrolyzers. As shown in Fig. 7a to 7c, the type of membrane directly determines the transmission path of ions between the anode and cathode of the electrolyzer. To better understand how membrane properties impact the efficiency and selectivity of CO₂RR, it is necessary to investigate the properties of the membrane, including chemical construction, the concentration of functional groups in a membrane, film thicknesses, water absorption capacity, and ionic conductivity, etc.⁸¹

4.1 Cation exchange membranes (CEMs)

As depicted in Fig. 7a, CEMs can promote cation flow from the anolyte to the catholyte. In 2008, Delacourt et al.⁸² first evaluated CO₂ reduction activity based on a CEM-based flow cell using a Nafion membrane and a direct supply of gas-phase CO₂. When 1 M KHCO₃ solution as a mildly basic buffer layer was passed between the membrane and the cathode GDE, the FE

of CO reached about 80% at 20 mA cm⁻² and about 20% at 100 mA cm⁻². Without adding the buffer layer, CO₂ was hardly reduced and the FE of H₂ was 100% at 20 mA cm⁻². Nevertheless, stable electrolysis could not be maintained for more than an hour. The main reason was the electrode poisoning at the interface of the Nafion membrane and the change in the electrolyte properties. In addition, more protons diffuse from the anode electrolyte to the cathode electrolyte, which would facilitate H₂ production and weaken the selectivity of CO₂ reduction. The above results prove the significance of aqueous electrolyte and ion management in gas flow cells that are essentially related to the selection of membranes.

The choice of ion exchange membranes must be considered in conjunction with the selection of catalysts, the selection of electrolytes and the target CO₂RR products. CEMs are commonly used for CO₂ reduction to form formic acid or formate because these cation exchange membranes can prevent the product of formate anions from passing through to the anode compartment, thereby preventing the loss of formic acid product. In addition, the CO product distribution can also be adjusted by cation exchange membrane during CO₂ electroreduction process.⁸³⁻⁸⁶ Considering that CEM may be a proton exchange membrane, such as Nafion, the proton concentration must be managed by choosing an acidic anode electrolyte. Another consideration for CEMs is that the excess of protons will elevate the hydrogen production on the cathode.

Modeling and simulation have proven to be well-established tools for studying performance-related issues of proton exchange membrane reactors.⁸⁷⁻⁸⁸ The most commonly used perfluorosulfonic acid (PFSA)-based membranes, such as Nafion, where sulfonic acid groups are fixed to the polymer backbones, are typically used for CO₂ reduction. These membranes

have strong acidity and high ionic conductivity due to the presence of sulfonic groups.⁸⁹ However, PFSA membranes have several known failure modes during cell operation, involving mechanical, thermal, and electrochemical processes. The most cited cause of membrane failure is chemical degradation.⁹⁰⁻⁹¹ Xie et al. deduced the degradation model of PFSA films based on the decompression mechanism and the backbone fracture at side chain positions, leaving the COOH group adhere to the remaining fragments.⁹² However, this model does not describe the formation of peroxides and free radicals, the effects of operating conditions, and the transport phenomena in the membrane electrode assembly. Later, Walsh and his colleagues simulated the degradation of perfluorinated ion-exchange membranes using conservation principles in a model containing a detailed description of the transport phenomena.⁹³ The results showed that the degradation process takes place by unzipping of the main chains and splitting of the side chains, and the numerical code is very effective.

Hydrocarbon-based membranes have attracted intensive interest as an alternative design, because they may be easier to manufacture than fluorine-based membranes. By adding the sulfonyl group ($-S(=O)_2-$) into different positions of benzenesulfonic acid, Fukushima et al constructed and evaluated the activation and stability energies of deprotonation reactions of these model molecules.⁹⁴ It is revealed that the activation energy decreases and the stabilization energy increases when a sulfonyl group is introduced between the carbon and sulfur atom of the sulfonyl group ($-SO_3H$). The results indicated that the introduction of highly electronegative functional groups can improve the performance of the hydrocarbon-based film without fluorine atoms.

4.2 Anion exchange membranes (AEMs)

Unlike CEMs, anion exchange membranes (AEMs) regulate the flow of anions (e.g., hydroxide) from the catholyte to the anolyte. As shown in Fig. 7b, the AEM may be better suited for CO₂RR than the CEM because of the encouragement of the CO₂ reduction and the prevention of H⁺ ion migration to the cathode to decrease the competitive HER. In fact, OH⁻ ions can quickly react with existing CO₂ to generate HCO₃⁻ and CO₃²⁻. It is inevitable that AEMs can facilitate the transport of all these anions from the catholyte to the anolyte. However, the ion flow rates of HCO₃⁻ and CO₃²⁻ are much lower than that of OH⁻, and the aggregation of these large anions will prevent the further migration of OH⁻ ions, thus reducing CO₂ reduction efficiency. **Furthermore, aqueous bicarbonate is a commonly used catholyte.** They can diffuse into the anolyte through the AEM, lower the pH for oxidation process and thereby reduce the efficiency of the anode. What's more, the crossover rate of products from catholyte to anolyte is likely to boost especially for anionic products (like formate) and neutral products (like methanol).⁹⁵ **In addition, AEM may be susceptible to excessive OH⁻ degradation, especially when the membrane has insufficient moisture.** An ideal AEM requires high ionic conductivity, high ion mobility and low permeability of products, thereby improving the kinetic transport of ions during CO₂ electrolysis, inhibiting the H₂ formation as a competitive reaction, and improving the overall performance of the device. **Up to now, many of the best-known membranes for CO₂ electroreduction electrolyzers use AEMs.**^{34, 73, 96-100}

Wang et al.¹⁰¹ synthesized a series of hydroxide-conductive polymers as the AEM materials to evaluate the efficiency and selectivity of the electrochemical CO₂ reduction (Fig. 7d). They indicated that using the AEM containing thiophene groups delivers superior CO₂RR catalytic performance with 71.5% formate FE at -1.64 V vs. saturated calomel electrode, far exceeding

that of the dimethyloctanal and hydroxybenzyl based membranes and the commercial Nafion 212 membrane (Fig. 7e-7f). The reason is that the membrane with thiophene functional groups exhibits an excellent high ionic conductivity, ion transport number and low formate permeability, which can improve the dynamics of ion transport during CO₂ electrolysis, inhibit the H₂ evolution, and weaken formate product crossover, contributing to cell performance improvement.

Recently, Sargent and co-workers presented a catalyst:ionomer bulk heterojunction architecture using an AEM-based flow cell that could achieve a partial ethylene current density of 1.3 A cm⁻² with cathodic energy efficiency reaching 45%.⁹⁷ The authors noted that the supplemental humidification gas CO₂ in the reactor demonstrates the importance of sufficient hydration during the vapor phase reduction process. The excellent performance of using an AEM flow electrolyzer for electrocatalytic CO₂ reduction paves the way for the realization of renewable electrochemistry for hydrocarbon production under large current densities required for industrial applications.

4.3 Bipolar membranes (BPMs)

In a bipolar membrane (BPM), the anion and the cation exchange layers are connected at the interfacial layer to catalyze the self-dissociation of water into H⁺ and OH⁻, which are selectively run to the cathode and the anode under reverse bias conditions (Fig. 7c). Compared with CEMs and AEMs, the obvious advantage of the BMPs is that they can maintain a constant pH value in the cathodic compartment and anodic compartment of the electrolytic cell, so that each half-reaction can independently select the ideal pH conditions. **At this point, this design may allow a wider choice of catalysts and the use of low-cost abundant metals instead of precious ones.**¹⁰²

BPM electrolyzers have been flexibly designed for use in flow batteries¹⁰³, fuel cells¹⁰⁴⁻¹⁰⁵, water electrolysis¹⁰⁶⁻¹⁰⁸, CO₂ separation¹⁰⁹ and CO₂ electroreduction¹¹⁰.

In 2016, Mallouk and co-workers displayed the application of a BPM based on a gas-phase CO₂ flow cell.³⁵ They demonstrated that the BPM-based cells can perform high current densities and stable operation, comparable with the equivalent CEM- or AEM-based devices. Later, they also reported a series of studies on the application of BPMs in electrochemical CO₂ reduction.^{79, 111-112} They reported a high stability of CO production for 24 h at a current density of 100 mA cm⁻² and a cell voltage of 3.4 V, with the Faradaic efficiency of approximately 65% in a CO₂ flow electrolyzer containing a BPM. Nevertheless, the current density with FE_{CO} of 50% is up to 200 mA cm⁻², which is the highest current density reported to date using a BPM at room temperature/pressure.⁷⁹ In addition, they found that the cross rate of formate was approximately 17 times lower for 3D or commercial BMP than that for commercial AEM under the same conditions (Fig. 7g).¹¹¹ The 3D and commercial BMPs have similar crossover rates of formate and methanol (Fig. 7h-7i). They manifested that ion crossover rates are limited by the degree of molecular penetration of BMPs rather than the interfacial areas of BMPs, and CEMs (like Nafion) are poor choices for preventing ion crossover.¹¹² Therefore, BMPs, especially 3D BMPs, are expected to become an integral part of CO₂ reduction flow electrolyzers to manufacture fuels and chemicals.

In general, it is more pronounced from the above examples that there is still a lot of rooms for improvement in terms of designing and synthesizing PEM materials. At the same time, in order to improve the performance of gas phase CO₂ flow electrolyzers, it is necessary to take catalysts, electrolytes, and target reduction products into a whole consideration.

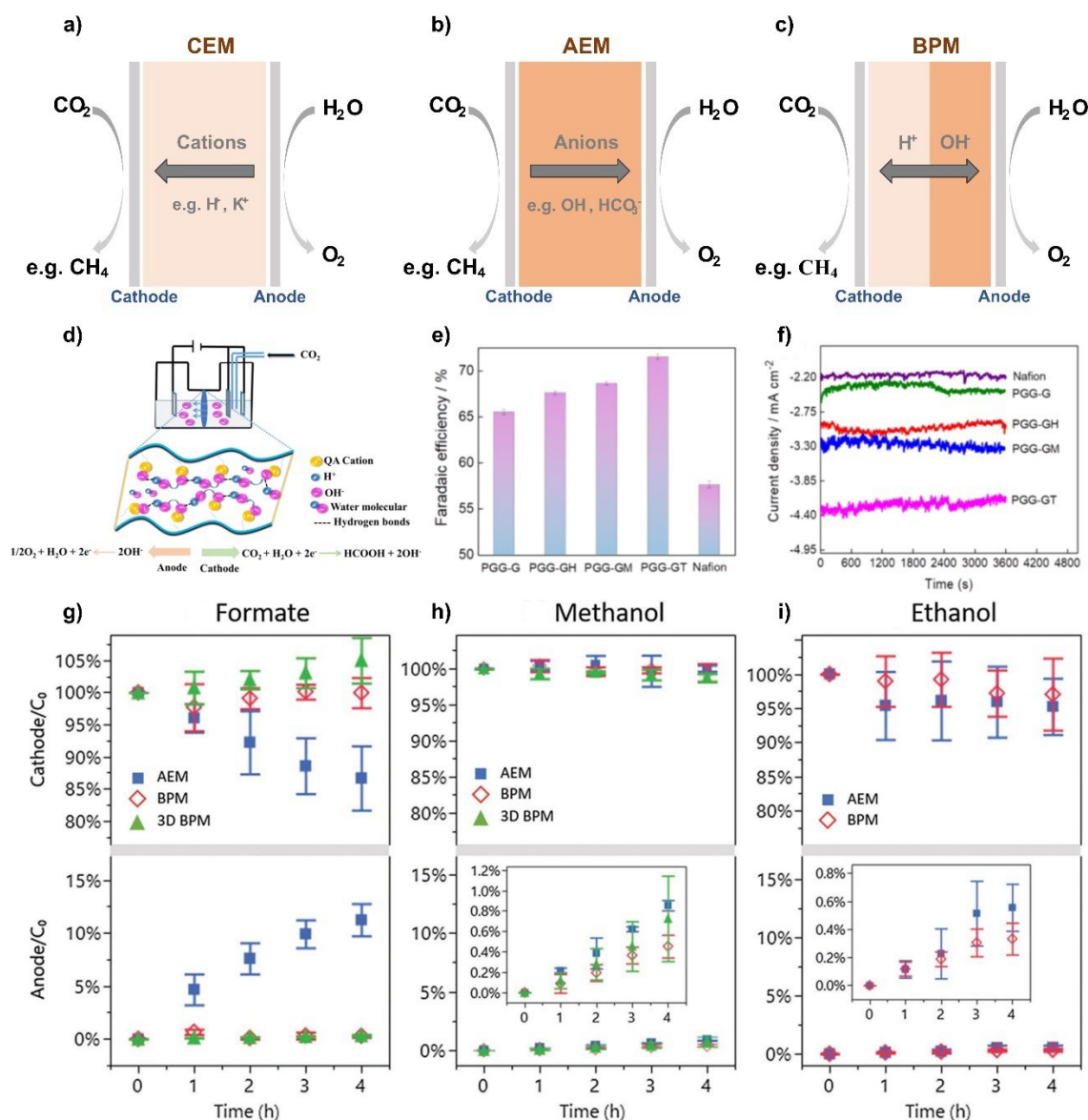


Fig. 7 Overview of ions transport pathways for three types PEM: (a) CEM, (b) AEM, and (c) BPM. (d) Schematic diagram of the electrochemical CO₂RR using chemically modified PGG membranes. (e) FEs and (f) current density of different membranes. Reproduced with permission.¹⁰¹ Copyright 2019, American Chemical Society. Crossover of (g) formate, (h) CH₃OH, and (i) C₂H₅OH vs. time in the AEM and BPM. Reproduced with permission.¹¹¹ Copyright 2018, Wiley-VCH.

5. Electrolytes

Electrolyte is another crucial part for electrocatalytic CO₂RR, and its main function is to conduct ionic charges between electrodes. The ideal electrolyte should possess but not limited to high solubility for CO₂, high ionic conductivity, high electrochemical stability, good

chemical compatibility with electrode materials, low viscosity of the electrolyte to ensure good CO₂ mass transfer from the bulk electrolyte solution to the electrode surfaces, easy operation and storage, and safety.^{16, 113-115} Thus, choosing the right electrolyte will be paramount for the performance of the electrochemical CO₂RR system, which can selectively and efficiently convert CO₂ into products.

5.1 Aqueous solutions

Liquid electrolytes are the most extensively employed electrolyte systems for CO₂ reduction. Among them, aqueous electrolyte systems have the advantages of low cost, large scale, wide availability, relatively easy preparation, safe handling and storage, and stable ionic conductivity, making them the most frequently used liquid electrolyte systems in research and practical applications. Moreover, aqueous solutions can act as both proton donors and proton acceptors to promote the formation of different electroactive substances. The pH, cations, anions, and concentrations of an aqueous electrolyte can affect the electrocatalytic CO₂ reduction performance.¹¹⁶⁻¹¹⁹

5.1.1 Cationic effects

Alkali metal cations in the electrolyte can affect the electrochemical CO₂ reduction activity and selectivity.¹²⁰⁻¹²¹ In 1991, Hori and Murata first demonstrated that the product selectivity of CO₂ and CO reduction on polycrystalline copper largely depends on the cationic species.¹²⁰ As shown in Fig. 8a, the selectivity of ethylene and alcohols products increases compared with that of CH₄ and H₂ with the increasing cation radius (Li⁺ < Na⁺ < K⁺ < Cs⁺). They explained that the smaller cations, the stronger the hydration capacities, and the more it can prevent the

propensity to adsorb on the electrode surface. Cations with larger ionic radii are more likely to adsorb on the electrode surface due to their lower hydration ability, making the CO₂ reduction potential move towards the positive direction of the outer Helmholtz layer. This reduced reduction potential leads to the decrease of proton concentration, resulting in a decrease of the selectivities towards CH₄ and H₂, which was consistent with the observed changes in hydrocarbon selectivity. Since then, several experimental reports and theoretical studies have confirmed and expanded the above observations.¹²²⁻¹²⁴ The cations adsorbed on the cathode surface can stabilize the negatively charged radical intermediate (*CO₂⁻), thereby decreasing H₂ evolution and facilitating CO₂ reduction, which can explain the gradual increase in the overall efficiency of CO₂ reduction with ionic size from Li⁺ to Cs⁺.¹²⁵ Notably, Koper et al provided definitive evidence that partially desolvated metal cations from electrolytes stabilize the *CO₂⁻ intermediate via a short-range local electrostatic interaction.¹²⁶

However, there remain some debates about the conclusion of cation adsorption on the electrode. Recent theoretical work indicated that specific alkaline cation adsorption conditions were not applicable to the CO₂ reduction. Part of the reason is that the calculated reduction potential of the alkali cations on the transition metal electrodes is more negative.¹²⁷⁻¹²⁸ Given the complex properties of the electrochemical interface, it is difficult to accurately tell the degree of interaction between the alkali ions and the electrode surface. The experimental investigation of the mechanism by which the specific cationic adsorption and/or non-specific interactions affect the surface electrochemical processes is challenging,¹²⁹ but it can determine the effect of cations on or in the vicinity of the electrode surface on the CO₂ reduction performance. The latest research results of Sargent et al show that enriching K⁺ near the

electrochemically active sites by a cation-augmenting layer can accelerate CO₂ activation, thereby effectively reducing CO₂ in strong acid.¹³⁰ In addition, the cation-augmenting layer allows cations (such as H⁺ and K⁺) to migrate from the electrolyte to the catalyst surface while slowing the outward diffusion of OH⁻, resulting in higher surface pH, which was favorable for C-C coupling.

5.1.2 Anionic effects

The anionic effects on CO₂ reduction activity and selectivity have been proposed to be dependent on pH value, buffer effect, and specific adsorption of anions on the surface of the cathode electrode.^{68, 131-133} Hori and colleagues investigated the effect of pH and pointed out significant differences in the C₂H₄/CH₄ production ratio among different anions in the electrolyte: the ratio of 4.16 in K₂SO₄ and 3.74 in KCl were higher than that of 1.02 in KHCO₃ and 0.11 in K₂HPO₄ (Fig. 8b).¹³⁴ In agreement with these studies, Mo and co-workers also confirmed that the enhanced selectivity for ethylene with suppressed HER is partially attributed to the higher local pH for promoting OH⁻ adsorption on catalyst.¹³⁵ Due to the release of OH⁻ during the electroreduction process, the electrolyte with low buffer capacity (K₂SO₄/KCl < KHCO₃ < K₂HPO₄) fails to neutralize the formed OH⁻ and thus enhances the local pH value of the non-equilibrium local area near the electrode, which is beneficial to CO₂ reduction over HER and C₂₊ over C₁ products. The maximum ethylene FE values in 0.1 M K₂HPO₄, KHCO₃ and K₂SO₄ solutions are 31.2%, 68.5% and 83.2%, respectively, which is also the highest ethylene FE reported.¹³⁵ In addition, other studies have also shown that the productions of H₂ and CH₄ increase as the concentration of KHCO₃ anions increases, again due to the local pH effects.¹³⁶

There are several challenges in studying the pH effects on CO₂ reduction. Considering the formation of CO₃²⁻ and HCO₃⁻ when CO₂ is purified in alkaline solutions, the electrolytes used for CO₂RR are usually limited to electrolytes with neutral or acidic pH values. Initial work by Tanaka et al. manifested the effect of pH on the formation of CO and HCOO⁻ towards electrochemical CO₂ reduction.¹³⁷ To gain an insight into the further-reduced product pathway, the pioneering work by Hori and co-workers showed that the product selectivity of CH₄ and C₂H₄ in electrochemical CO reduction reaction was affected by pH.^{124, 138-139} Weitzner et al. used a recently developed effective screening medium method and density functional theory to illustrate the effect of pH on the binding energy of CO.¹⁴⁰ They found that the interdependent voltage and pH value would lead to a special change in adsorption site favoring the CO binding on Cu (100) terraces, making it a multi-coordinated bridge or hollow positions. These findings also provide a physical basis for the recent *in-situ* spectroscopic observation of the CO₂RR process in alkaline media. Wang and co-workers developed an *in-situ* Raman flow electrolytic cell for the experimental study on local pH changes near the GDE during the CO₂ reduction process under working conditions (Fig. 8c).¹⁴¹ They proved that at the interface between the cathode electrode surface and the electrolyte, CO₂ reacts with the alkaline KOH solution to form CO₃²⁻ and HCO₃⁻, thus making the local environment of the electrode surface close to neutral (Fig. 8d-8e). In addition, due to the Nernst potential of the pH gradient layer at the cathodic electrode/electrolyte interface, the use of the alkaline electrolyte results in a nominal overpotential drop. With the increase of CO₂ reduction current density, the neutralization reaction between CO₂ and OH⁻ still exists, but the pH gradient layer will be narrowed.

It is noted that pH value is a significant factor in determining CO₂ reduction products and is correlated with catalytic activity and selectivity. Bell et al. elucidated that the composition and concentration of electrolyte anions (such as perchlorates, sulfate, bicarbonates, borates, and phosphates) had negligible effects on the formation of CO, formic acid, ethylene, and ethanol, but notably affected the formation of CH₄ and H₂, which highly relied on the pH of the electrolytes.¹³¹ Recent works have also improved the mechanistic understanding of pH effects for CO₂RR.^{116, 142} As shown in Fig. 8f to 8h, the absolute molar formation rate and Faradaic efficiency of products for CO₂ reduction plotted versus normal hydrogen electrode (NHE) scale illustrates the pH effect.¹¹⁶ In view of the electrolysis experiments with high current density, the trend of HER directly corresponds to the local interface pH value. Meanwhile, during the reaction, the proton consumption causes the local pH of the low concentration bicarbonate to rise sharply and suppress HER. The exact pH of the interface also depends on the reduction current. They found that pH did not seem to be the only parameter controlling CH₄ formation. Unlike the generation of H₂ or CH₄, the CO formation is independent, and has a decoupled electron transfer mechanism.

The electrolytes with higher pH values favor the activity and generation of C₂₊ products at a lower applied potential (especially for copper catalysts).^{73, 143} Wang et al. compared the C₂₊ product formation rates on F-Cu catalyst under different concentrations of KOH solution. As shown in Fig. 9a, the formation rate of C₂₊ was as high as 3,050 μmol h⁻¹ cm⁻² at -0.62 V vs. RHE in 2.5 M KOH solution. However, the lower the concentration of KOH, the lower the formation rate of C₂₊ under the same potential.⁶³ **In this vein, further boosting the selectivity and FE of C₂₊ products by KOH electrolyte is also a direction worthy of in-depth study.** The

specific adsorption of anions on the cathode can have a significant effect on the activity and selectivity of CO₂ reduction as well.^{68, 144} Especially, the halogen ions adsorbed on the cathode surface can change the electronic structure of the catalysts, thus affecting the interaction between the cathode surface and active intermediates to promote the formation of CO₂RR.^{63, 145-148} There is evidence that when the KHCO₃ electrolyte solution contains halide ions, with the increase of halide ionic radius from Cl⁻ to I⁻, the current density of CO₂ reduction increases gradually, but the Faradaic efficiency of C₂₊ products remains unchanged (Fig. 9b-9c).¹⁴⁷⁻¹⁴⁸ Wang et al. also confirmed the above view that when KX (X = F, Cl, Br, and I) was added to the electrolyte, the current density and the formation rate of C₂₊ products increased with the decrease of the halogen electronegativity, while the C₂₊ FE only changed slightly.⁶³ However, it remains unclear which anion factor has the dominating influence on the CO₂RR and this represents another field of future research aiming at deeper understanding of the ion interactions in CO₂ reduction process.

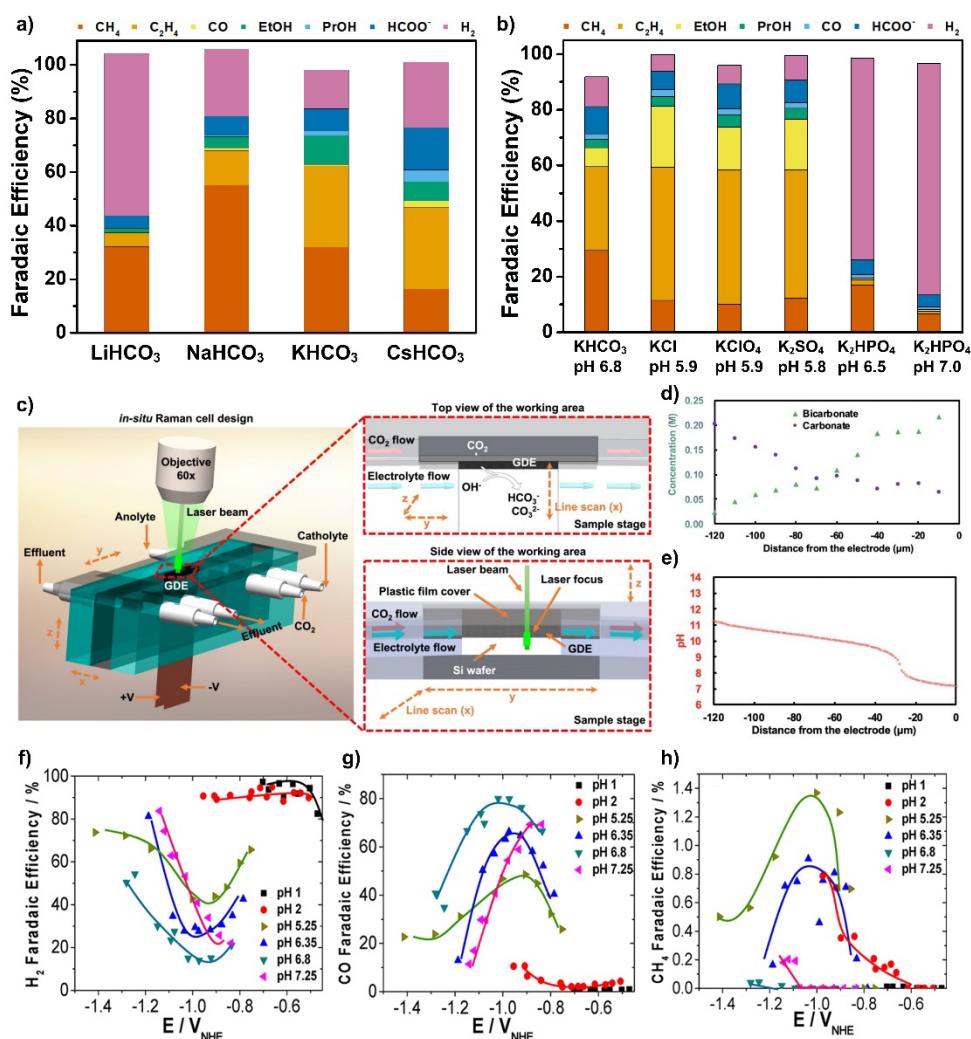


Fig. 8 (a) Effect of cationic species on FEs of various products. Reproduced from the data.¹²⁰ Copyright 1991, The Chemical Society of Japan. (b) Effect of anionic species on FEs of various products. Reproduced from the data in Horii et al (1989).¹³⁴ (c) Designed flow cell for performing *in-situ* Raman measurements under continuous-flow CO₂ reduction. (d) HCO₃⁻ and CO₃²⁻ concentrations, and (e) pH profile with respect to distance from GDE surface. Reproduced with permission.¹⁴¹ Copyright 2020, American Chemical Society. FE for (f) H₂, (g) CO, and (h) CH₄ in CO₂-saturated electrolytes with different pH values. Reproduced with permission.¹¹⁶ Copyright 2018, American Chemical Society.

5.2 Organic solvents

The solubility of CO₂ in DMF, propyl carbonate, CH₃OH, DMSO, and acetonitrile is approximately 20, 8, 5, 4 and 4 times higher than that in water at ambient conditions, respectively (Fig. 9d).¹⁶ The main advantages of using non-aqueous electrolytes for CO₂RR are

that they 1) have higher CO₂ solubility than aqueous electrolytes; 2) suppress the unwanted HER through limited proton transfer; 3) allow selective reaction pathways conducive to the formation of the target products.^{3, 7, 149-151} Machan and co-workers reported that a nonaqueous acetonitrile flow cell had a CO selectivity of over 80% and achieved current densities higher than 50 mA·cm⁻². The flow configuration experiments in DMF solution showed greatly increased current activity relative to the H-type cell.¹⁵²

Some studies have investigated CO₂ reduction in mixed electrolytes that allow tuning proton concentrations and avoid precipitation of carbonate.¹⁵³⁻¹⁵⁶ Hori et al. showed that with increasing water content in acetonitrile, CO₂ reduction was more favorable to the generation of formic acid than oxalic acid.¹⁵³ Kus and co-workers also indicated that due to the presence of a handful of protons in the acetonitrile-water electrolyte solution, the formation of CO dominated over formic acid. This implies that the selectivity of product formation can be tuned by the composition of the electrolyte solution.¹⁵⁴

Unfortunately, although most organic solvents can significantly inhibit HER, they usually exhibit inefficient FE during the CO₂RR. Additionally, organic solvent electrolytes also have many intrinsic disadvantages, including their high cost, volatility, flammability, toxicity, and the potential miscibility with reductive products.¹⁵⁷⁻¹⁵⁸ These greatly limit the prospects of organic solvent electrolytes for CO₂ reduction in large-scale practical applications.

5.3 Ionic liquids

Ionic liquids are a class of ionic compounds with specific structures, which usually present a liquid state at atmospheric temperature. They have been widely applied to supporting systems of versatile electrochemical reactions, such as organic electrochemical synthesis¹⁵⁹ and

electrocatalytic reactions¹⁶⁰. Ionic liquids usually have appreciable electric conductivity, good thermochemical stability, low vapor pressure, and wide operating potential window, which make them superior to traditional aqueous electrolyte and organic electrolyte systems.¹⁶¹ In addition, due to the existence of ion exchange fields, ionic liquids are recognized to have high CO₂ solubility under ambient pressure and temperature. Therefore, researchers continue to innovate and try to use ionic liquids to improve the performance of electrocatalytic reduction of CO₂ to produce high value-added products.

Some studies believe that certain ionic liquids are both electrolytes and promoters for CO₂ activation. In 2011, Rosen et al. first reported that an ionic liquid ([EMIM][BF₄]) can combine with the *CO₂ intermediates to form complexes and significantly decrease the energy barrier and the overpotential of the CO₂ activation in the reduction process (Fig. 9e).¹⁶² Then, Shi and co-workers reported that the highest CO Faradaic efficiency delivered 90.1% at -1.72 V vs. Pt wire on Ag cathode owing to the high solubility of CO₂ in the [Bmim][CF₃SO₃]/PC non-aqueous electrolyte. No poisonous species were observed on the cathode during the 3 h electrolysis process.¹⁵⁵ In addition, they also obtained that [Bmim]⁺ was absorbed on the Au electrode to form ionic liquid film. The generated CO₂⁻ radical interacted with [Bmim]⁺ to induce the formation of [Bmim-CO₂]. Thus, the activation energy and overpotential of CO₂ electrochemical reduction were reduced through this route.¹⁶³ As shown in Fig. 9f, Lim and co-workers also further conducted systematic experimental studies to demonstrate that the cations and anions of the ionic liquids can combine and stabilize reaction intermediates, thereby forming a suitable microenvironment to reduce energy barriers and improve reaction kinetics.¹⁶⁴

Miller and co-workers¹⁶⁵ reported a series of new ruthenium complexes for kinetic comparison, which provided a platform for understanding how strong *trans* effect ligands and redox-active ligands work together to achieve rapid electrochemical reduction from CO₂ to CO in an acetonitrile electrolyte containing tetrabutylammonium hexafluorophosphate (TBAPF₆) at moderate potential. Etzold et al. used a [BMIm][NTf₂] ionic liquid as the chemical trapping agent to react with one or more intermediates to explore the mechanism of CO₂ reduction.¹⁶⁶ They found that the presence of the ionic liquid can notably alter the product range by selectively inhibiting the production of C₂H₄, C₂H₅OH, and n-C₃H₇OH without interfering Faradaic efficiency or partial current density of the products. Ethane is reconsidered to be formed through an independent pathway involving a CO dimerization process, rather than a reduction product that has long been considered to re-adsorb ethylene during CO₂RR. Considering the huge structural flexibility in ionic liquids, it is feasible to selectively interact with intermediates by elaborately designing task-specific ionic liquids to recognize the reaction paths of CO₂ reduction products.

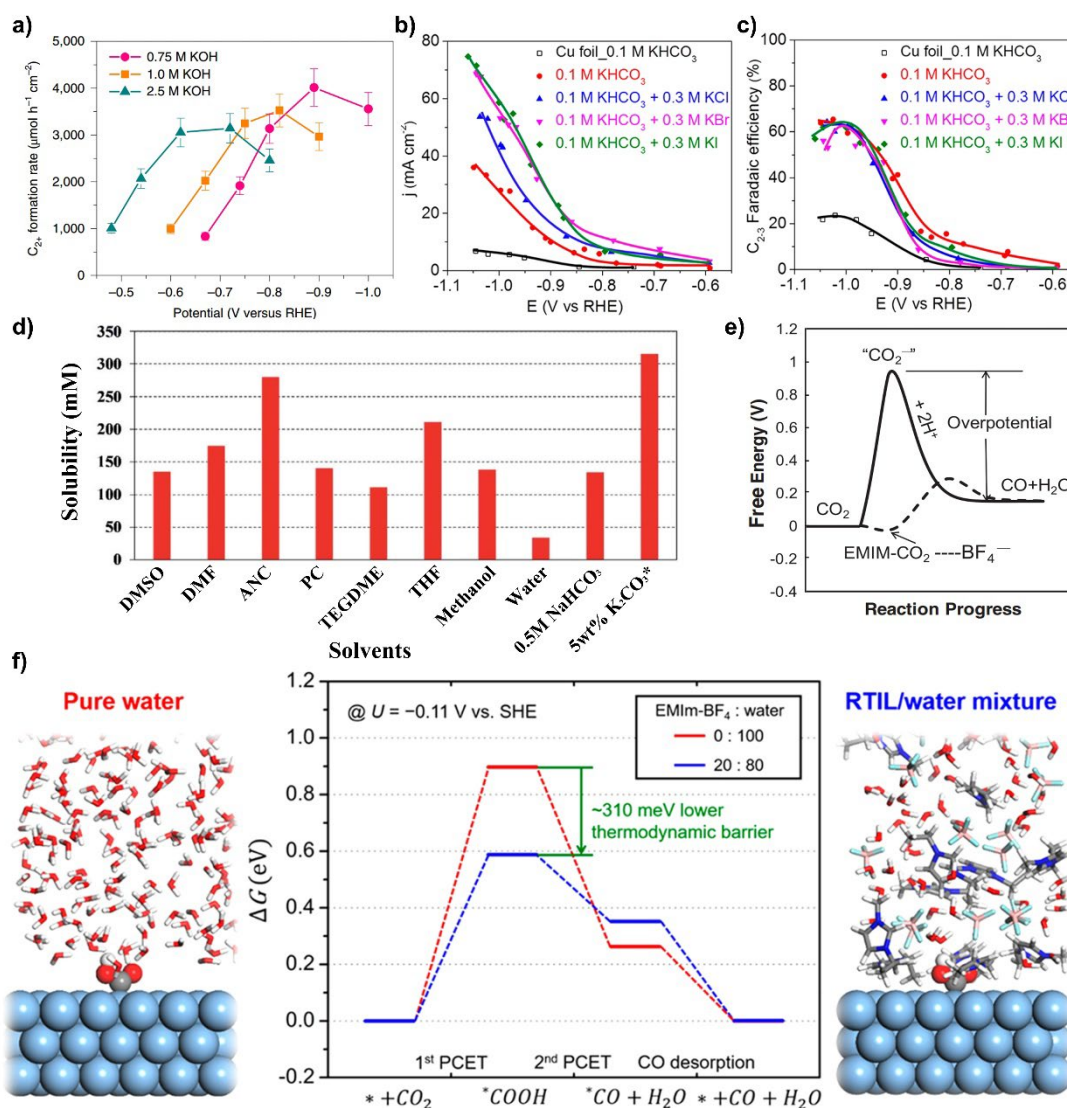


Fig. 9 (a) The formation rates of C₂₊ products in different concentrations of KOH. Reproduced with permission.⁶³ Copyright 2020, Springer Nature. (b) Current density and (c) total FE of C₂₊ products in different electrolytes. Reproduced with permission.¹⁴⁷ Copyright 2017, American Chemical Society. (d) The solubility of CO₂ in various organic solvents. Repainted with permission.¹⁶ Copyright 2020, Royal Society of Chemistry. (e) A schematic of how the free energy of the system changes in water and ionic liquids. Reproduced with permission.¹⁶² Copyright 2011, American Association for the Advancement of Science. (f) Calculated reaction free energy profiles in ionic liquids/water mixed electrolytes. Reproduced with permission.¹⁶⁴ Copyright 2018, American Chemical Society.

5.4 Solid-state electrolytes

In CO₂RR systems, solid-state electrolytes have recently been developed as promising alternatives to conventional liquid electrolytes. Compared with the dissolved solutes in a

traditional liquid electrolyte (for example, the frequently used KHCO_3 solution), these ion-conducting solid polymers can help electrogenerated cations or anions shuttle to form pure products and avoid mixing with conventional electrolytes. Wang and co-workers elucidated for the first time the use of a solid electrolyte device for electrocatalytic CO_2 reduction to continuously produce ultrahigh-purity liquid fuel productions.¹⁶⁷ As illustrated by the schematic in Fig. 10a, porous solid-state electrolyte (SSE) conductors were placed between the tightly contacting AEM and CEM membranes to effectively transmit the electrogenerated ions and notably reduce the ohmic loss of the whole equipment. It is worth noting that the cathode GDL is completely separated from the solution medium, which would not cause the flooding issue of the GDE, thus greatly guaranteeing operation stability even under the large negative overpotential for high catalytic currents. They successfully demonstrated the use of the device to generate pure formic acid solutions with a high concentration of 12.1 M and exhibited a continuous and stable preparation of ~ 0.1 M HCOOH with selectivity of more than 80% for 100 h. Moreover, other types of liquid product fuels such as CH_3COOH , $\text{CH}_3\text{CH}_2\text{OH}$, $\text{CH}_3\text{CH}_2\text{CH}_2\text{OH}$, were also obtained using solid electrolytes-based flow cell by adjusting the catalyst. There is no doubt that this solid electrolyte electrolyzer provides the opportunity for effective separation of CO_2 reduction products and diminish the cost of product separation process. However, there are still several challenges that hinder its actual production: the limited concentration of the product, the low production rate for industrial applications, and the use of liquid electrolytes for the oxidation reaction.

Wang et al. subsequently improved the anode inlet system based on such a solid electrolyte cell, and proposed an all-solid-state reactor for electrochemical CO_2 reduction.¹⁶⁸ Notably, they

used a humidified gaseous stream H_2 for the hydrogen oxidation reaction rather than a liquid acid for the water oxidation (Fig. 10b). They proved the generation of the nearly 100 wt% high-purity formic acid solutions using a highly active, selective, and stable Bi catalyst through the all-solid-state electrochemical system, which opens the possibility for all-solid-state electrolyzers to be suitable for modular and high-pressure systems in future large-scale deployments.

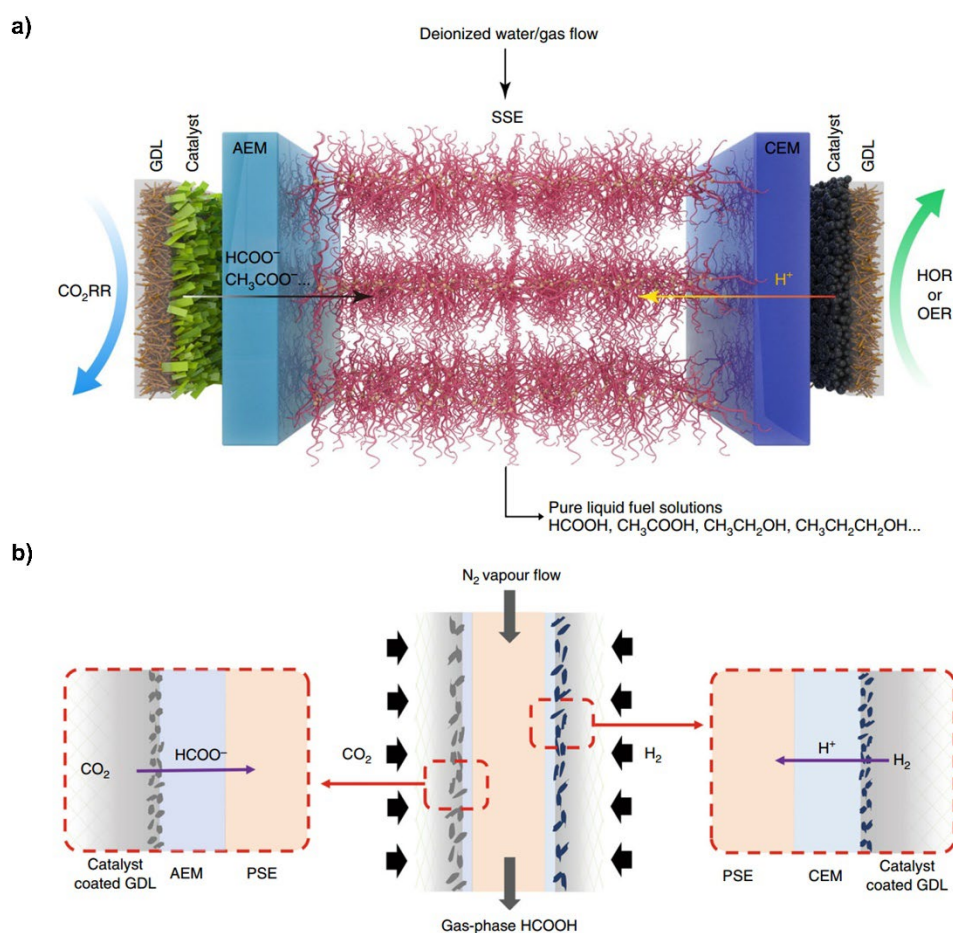


Fig. 10 (a) Schematic illustration of the CO_2 reduction reactor with solid electrolyte. Reproduced with permission.¹⁶⁷ Copyright 2019, Springer Nature. (b) Schematic illustration of the all-solid-state electrochemical CO_2RR to formic acid reactor.¹⁶⁸ Copyright 2020, Springer Nature.

6. Conclusion

As a clean and sustainable technology for the future, electrochemical CO₂ reduction technology is making strides in the search for catalyst design innovation and reactor system engineering. The efficiency and product selectivity of CO₂RR are not only determined by electrocatalysts but also affected by the electrolyzer configuration to a large extent. The continuous flow CO₂ cell under development increases the likelihood of large-scale CO₂ reduction processes because such configuration allows the direct injection of exhaust CO₂ into the cell. In this review, we have examined in detail the current impacts of noncatalyst units and feedstock properties on the overall CO₂ reduction performance of flow cells, including reactor design, flow field, reactants supply, electrode structure, membranes, and electrolyte effects, **summarizing the characteristics, superiorities, and obstacles of the electrolyzers (Table 1)** and providing valuable insights into the real-world CO₂ electrolysis for industrial applications. It is necessary to optimize multiple parameters and reaction systems simultaneously to effectively carry out continuous flow CO₂ electroreduction. Several main aspects to focus in the near term include:

(1) Simultaneous use of continuous CO₂-saturated electrolyte and vapor-phase CO₂ flow to mitigate mass transfer limitations, and optimize humidity, flow rate of the reaction gas flow, and flow field related to the concentration of CO₂ on the electrode surface.

(2) Further optimization of membrane reactors by utilizing the membrane technologies that have been developed and applied in commercial fuel cells and water electrolyzers to guide the optimal integration of ion exchange, conductivity and water transfer characteristics in CO₂ reduction systems.

(3) Regulating the appropriate wetting properties of the GDE by loading hydrophobic components and further understanding of the influence of electrolyte interactions on the CO₂ reduction process.

(4) Further development of all-solid-state electrochemical systems to facilitate the direct generation of pure liquid products from all-solid-state reactors for future large-scale deployments.

(5) The establishment of a computation model for rational design of the electrolytic cell structure. In this context, numerical simulations will be used to elucidate the effect of flow rate and novel flow field on CO₂ conversion and consumption rate for the optimization of the reactor performance.

In summary, lab-scale continuous flow electrolyzers provide the opportunity to reduce CO₂ and have received increasing attention in recent few decades. They will be one of the major development directions in the future for carbon neutralization. While many challenges remain for flow electrochemical CO₂ reduction at the current stage, it is believed that with continued in-depth research and development to optimize and improve the electrolyzer configuration, the industrial scale CO₂ electrolysis for clean fuel and value-add chemicals will be realized in the near future.

Table 1. Summarize of superiorities and obstacles of different reactors and components for CO₂RR.

Reactor types/Components		Characteristics	Superiorities	Drawbacks
H-type cell	Conventional H-type cell	Batch reactor	Commercially available; Screening electrocatalysts; Wide range of electrode selections; Convenient operation	Limitation on the detection of trace liquid products; Limitation of mass transport; Difficulty in the large-scale application
Flow cell	Membrane-based flow cell	Polymer electrolyte membrane configuration; Circulating CO ₂ -saturated electrolyte	Controlling reactant delivery; Fundamentals of commercial application design; Lower cell resistance; Higher mass transport; Detection of low concentration products; Accurate voltage measurement	The strong corrosion by the high overpotentials
	Microfluidic flow cell	Gas phase CO ₂ ; Flow channel; A membrane-free cell	Higher mass transport; Flexibility in operation conditions; Minimization of the pH decrease; Avoiding the high membrane cost; Mitigating water management; Allowing use of strong alkaline electrolyte	Prone to product re-oxidation; Lower liquid products concentration
	A cell with gapless electrode	Presses two electrodes together with an ion-exchange membrane in between	Higher mass transport; Lower ohmic losses; Larger catalytic current density; Able to provide different types of surface ion environment; Decreasing risk of catalyst poisoning; Easy to pressurize the reactant flow and enhance the local CO ₂ concentration	Blocking the active site by the liquid products flooding back to the gas-diffusion electrode; A great challenge for scale-up application by the pressure sensitive resulting from different pressure across the membrane
Membranes	Cation exchange membrane (CEM)	Allowing for the passage of cations while preventing the anions	Widely used; Preventing the loss of formic acid product	Facilitating H ₂ production and weakening the selectivity of CO ₂ reduction

	Anion exchange membrane (AEM)	Allowing for the passage of anions while preventing the cations	Blocking proton transfer, suppressing the hydrogen evolution reaction (HER), and promoting CO ₂ reduction; Using low-cost non-precious metals for oxygen evolution reaction	Easily degradation by excessive OH ⁻ ; Preventing the further migration of OH ⁻ ions due to the aggregation of large anions (e.g., HCO ₃ ⁻ and CO ₃ ²⁻)
	Bipolar membrane	Formed by lamination or close contact of AEM and CEM; Operated in either forward bias mode or reverse bias mode	Better control of pH; Independently selecting the ideal pH conditions of each half-reaction; Wide choice of catalysts; Limitation of ion crossover rates; Using low-cost abundant metals instead of precious ones	Driving up the voltage required to drive electrolysis and reducing overall energy efficiency by developing the large membrane potential under reverse bias
Electrolytes	Aqueous solution	Water solvent	Low cost; Large scale; Wide availability; Easy preparation; Safe handling and storage; Stable ionic conductivity	Low CO ₂ solubility and utilization rate; Difficult and costly to recover products from liquid electrolyte
	Organic solvent	Organic solution	Higher CO ₂ solubility; Suppressing the HER; Allowing selective reaction pathways conducive to the formation of the target products	High cost; Volatility; Flammability; Toxicity; Potential miscibility with reductive products; Inefficient Faradaic Efficiency
	Ionic liquid	Ionic compounds	Appreciable electric conductivity; Good thermochemical stability; Low vapor pressure; Wide operating potential window; Higher CO ₂ solubility; Structural flexibility	High viscosity to limit CO ₂ diffusion rate; Low current density
	Solid-state electrolyte	Ion-conducting solid polymers	Helps electrosynthesize pure products without mixing with conventional electrolytes	Low production rate

Conflicts of Interest

There are no conflicts of interest to declare.

Acknowledgements

The authors acknowledge the financial support of this work by the Science, Technology, and Innovation Commission of Shenzhen Municipality (Program Nos. JCYJ20180508151856806 and RCBS20200714114818140), the Research Grants Council of the Hong Kong Special Administrative Region, China (Project No. PDFS2122-5S02), The Hong Kong Polytechnic University (Project No. ZE2F, YWA1 and YW5B), the Fundamental Research Funds for the Central Universities (No. G2020KY05129), and the China Postdoctoral Science Foundation (2019M663118).

References

1. S. Chu and A. Majumdar, *Nature*, 2012, **488**, 294-303.
2. P. Prabhu, V. Jose and J. M. Lee, *Adv. Funct. Mater.*, 2020, **30**, 1910768.
3. J. Qiao, Y. Liu, F. Hong and J. Zhang, *Chem. Soc. Rev.*, 2014, **43**, 631-675.
4. K. Elouarzaki, V. Kannan, V. Jose, H. S. Sabharwal and J. M. Lee, *Adv. Energy Mater.*, 2019, **9**, 1900090.
5. E. S. Sanz-Perez, C. R. Murdock, S. A. Didas and C. W. Jones, *Chem. Rev.*, 2016, **116**, 11840-11876.
6. A. N. Kuhn, H. Zhao, U. O. Nwabara, X. Lu, M. Liu, Y.-T. Pan, W. Zhu, P. J. A. Kenis and H. Yang, *Adv. Funct. Mater.*, 2021, **31**, 2101668.
7. S. Das, J. Pérez-Ramírez, J. Gong, N. Dewangan, K. Hidajat, B. C. Gates and S. Kawi, *Chem. Soc. Rev.*, 2020, **49**, 2937-3004.
8. L. Ye, H. Yue, Y. Wang, H. Sheng, B. Yuan, L. Lv, C. Li, B. Liang, J. Zhu and H. Xie, *Ind. Eng. Chem. Res.*, 2014, **53**, 10557-10565.

9. G. Wang, J. Chen, Y. Ding, P. Cai, L. Yi, Y. Li, C. Tu, Y. Hou, Z. Wen and L. Dai, *Chem. Soc. Rev.*, 2021, **50**, 4993-5061.
10. P. Daw, S. Chakraborty, G. Leitus, Y. Diskin-Posner, Y. Ben-David and D. Milstein, *ACS Catal.*, 2017, **7**, 2500-2504.
11. H. Li, C. Qiu, S. Ren, Q. Dong, S. Zhang, F. Zhou, X. Liang, J. Wang, S. Li and M. Yu, *Science*, 2020, **367**, 667-671.
12. X. Zhao, Y. Fan, W. Zhang, X. Zhang, D. Han, L. Niu and A. Ivaska, *ACS Catal.*, 2020, **10**, 6367-6376.
13. H. S. Jeon, J. Timoshenko, C. Rettenmaier, A. Herzog, A. Yoon, S. W. Chee, S. Oener, U. Hejral, F. T. Haase and B. R. Cuenya, *J. Am. Chem. Soc.*, 2021, **143**, 7578-7587.
14. S. Liang, N. Altaf, L. Huang, Y. Gao and Q. Wang, *J. CO₂ Util.*, 2020, **35**, 90-105.
15. D. M. Weekes, D. A. Salvatore, A. Reyes, A. Huang and C. P. Berlinguette, *Acc. Chem. Res.*, 2018, **51**, 910-918.
16. S. Garg, M. Li, A. Z. Weber, L. Ge, L. Li, V. Rudolph, G. Wang and T. E. Rufford, *J. Mater. Chem. A.*, 2020, **8**, 1511-1544.
17. Z. Sun, T. Ma, H. Tao, Q. Fan and B. Han, *Chem*, 2017, **3**, 560-587.
18. H. Shen, Z. Gu and G. Zheng, *Sci. Bull.*, 2019, **64**, 1805-1816.
19. C. Chen, Y. Li, S. Yu, S. Louisia, J. Jin, M. Li, M. B. Ross and P. Yang, *Joule*, 2020, **4**, 1688-1699.
20. T.-T. Zhuang, Z.-Q. Liang, A. Seifitokaldani, Y. Li, P. De Luna, T. Burdyny, F. Che, F. Meng, Y. Min, R. Quintero-Bermudez, C. T. Dinh, Y. Pang, M. Zhong, B. Zhang, J. Li, P.-N.

- Chen, X.-L. Zheng, H. Liang, W.-N. Ge, B.-J. Ye, D. Sinton, S.-H. Yu and E. H. Sargent, *Nat. Catal.*, 2018, **1**, 421-428.
21. C. Cao, D.-D. Ma, J.-F. Gu, X. Xie, G. Zeng, X. Li, S.-G. Han, Q.-L. Zhu, X.-T. Wu and Q. Xu, *Angew. Chem. Int. Ed.*, 2020, **59**, 15014-15020.
22. P. Wang, H. Yang, Y. Xu, X. Huang, J. Wang, M. Zhong, T. Cheng and Q. Shao, *ACS Nano*, 2021, **15**, 1039-1047.
23. P. Deng, F. Yang, Z. Wang, S. Chen, Y. Zhou, S. Zaman and B. Y. Xia, *Angew. Chem. Int. Ed.*, 2020, **59**, 10807-10813.
24. R. S. Jayashree, S. K. Yoon, F. R. Brushett, P. O. Lopez-Montesinos, D. Natarajan, L. J. Markoski and P. J. A. Kenis, *J. Power Sources*, 2010, **195**, 3569-3578.
25. D. T. Whipple, E. C. Finke and P. J. A. Kenis, *Electrochem. Solid ST.*, 2010, **13**, B109-B111.
26. S. Ma, M. Sadakiyo, R. Luo, M. Heima, M. Yamauchi and P. J. A. Kenis, *J. Power Sources*, 2016, **301**, 219-228.
27. T. T. H. Hoang, S. Ma, J. I. Gold, P. J. A. Kenis and A. A. Gewirth, *ACS Catal.*, 2017, **7**, 3313-3321.
28. H. Wang, D. Y. C. Leung and J. Xuan, *Appl. Energy*, 2013, **102**, 1057-1062.
29. X. Lu, D. Y. C. Leung, H. Wang and J. Xuan, *Appl. Energy*, 2018, **227**, 525-532.
30. X. Lu, D. Y. C. Leung, H. Wang and J. Xuan, *Renew. Energ.*, 2017, **102**, 15-20.
31. X. Lu, D. Y. C. Leung, H. Wang, M. M. Maroto-Valer and J. Xuan, *Renew. Energ.*, 2016, **95**, 277-285.
32. X. Lu, D. Y. C. Leung, H. Wang and J. Xuan, *Appl. Energy*, 2017, **194**, 549-559.

33. V. Kannan, K. A. Raman, A. Fisher and E. Birgersson, *Ind. Eng. Chem. Res.*, 2019, **58**, 19361-19376.
34. S. Ren, D. Joulié, D. Salvatore, K. Torbensen, M. Wang, M. Robert and C. P. Berlinguette, *Science*, 2019, **365**, 367-369.
35. Y. C. Li, D. Zhou, Z. Yan, R. H. Gonçalves, D. A. Salvatore, C. P. Berlinguette and T. E. Mallouk, *ACS Energy Lett.*, 2016, **1**, 1149-1153.
36. X. Wang, Z. Y. Wang, F. P. G. de Arquer, C. T. Dinh, A. Ozden, Y. G. C. Li, D. H. Nam, J. Li, Y. S. Liu, J. Wicks, Z. T. Chen, M. F. Chi, B. Chen, Y. Wang, J. Tam, J. Y. Howe, A. Proppe, P. Todorović, F. W. Li, T. T. Zhuang, C. M. Gabardo, A. R. Kirmani, C. McCallum, S. F. Hung, Y. W. Lum, M. C. Luo, Y. M. Min, A. N. Xu, C. P. O'Brien, B. Stephen, B. Sun, A. H. Ip, L. J. Richter, S. O. Kelley, D. Sinton and E. H. Sargent, *Nat. Energy*, 2020, **5**, 478-486.
37. B. Endrődi, G. Bencsik, F. Darvas, R. Jones, K. Rajeshwar and C. Janáky, *Prog. Energy Combust. Sci.*, 2017, **62**, 133-154.
38. A. Reyes, R. P. Jansonius, B. A. W. Mowbray, Y. Cao, D. G. Wheeler, J. Chau, D. J. Dvorak and C. P. Berlinguette, *ACS Energy Lett.*, 2020, **5**, 1612-1618.
39. W. Lee, Y. E. Kim, M. H. Youn, S. K. Jeong and K. T. Park, *Angew. Chem. Int. Ed.*, 2018, **57**, 6883-6887.
40. J. Wu, F. G. Risalvato, P. P. Sharma, P. J. Pellechia, F.-S. Ke and X.-D. Zhou, *J. Electrochem. Soc.*, 2013, **160**, F953-F957.
41. I. Merino-Garcia, J. Albo and A. Irabien, *Nanotechnology*, 2018, **29**, 014001.
42. Y. Chen, A. Vise, W. E. Klein, F. C. Cetinbas, D. J. Myers, W. A. Smith, T. G. Deutsch and K. C. Neyerlin, *ACS Energy Lett.*, 2020, **5**, 1825-1833.

43. M. Mehrpooya, M. Kheir Rouz and A. Nikfarjam, *Ind. Eng. Chem. Res.*, 2015, **54**, 3640-3647.
44. L. Yao, *Phys. Fluids*, 2019, **31**, 065107.
45. Y. Vazifeshenas, K. Sedighi and M. Shakeri, *Int. J. Hydro. Energy*, 2015, **40**, 15032-15039.
46. B. Ibrahimoglu, M. Z. Yilmazoglu and S. Celenk, *Fuel Cells*, 2017, **17**, 786-793.
47. D.-H. Wen, L.-Z. Yin, Z.-Y. Piao, C.-D. Lu, G. Li and Q.-H. Leng, *Int. J. Energy Res.*, 2017, **41**, 2184-2193.
48. X. Ke, J. M. Prah, J. I. D. Alexander, J. S. Wainright, T. A. Zawodzinski and R. F. Savinell, *Chem. Soc. Rev.*, 2018, **47**, 8721-8743.
49. C. R. Dennison, E. Agar, B. Akuzum and E. C. Kumbur, *J. Electrochem. Soc.*, 2015, **163**, A5163-A5169.
50. M. E. Leonard, L. E. Clarke, A. Forner-Cuenca, S. M. Brown and F. R. Brushett, *ChemSusChem*, 2020, **13**, 400-411.
51. J. Lee, J. Lim, C.-W. Roh, H. S. Whang and H. Lee, *J. CO₂ Util.*, 2019, **31**, 244-250.
52. K. Tüber, A. Oedegaard, M. Hermann and C. Hebling, *J. Power Sources*, 2004, **131**, 175-181.
53. S. Ressel, A. Laube, S. Fischer, A. Chica, T. Flower and T. Struckmann, *J. Power Sources*, 2017, **355**, 199-205.
54. K. M. Lisboa, J. Marschewski, N. Ebejer, P. Ruch, R. M. Cotta, B. Michel and D. Poulikakos, *J. Power Sources*, 2017, **359**, 322-331.
55. J. R. Hudkins, D. G. Wheeler, B. Peña and C. P. Berlinguette, *Energy Environ. Sci.*, 2016, **9**, 3417-3423.

56. V. Bandlamudi, P. Bujlo, V. Linkov and S. Pasupathi, *Fuel Cells*, 2019, **19**, 231-243.
57. G. Wang, L.-W. Feng, W. Huang, S. Mukherjee, Y. Chen, D. Shen, B. Wang, J. Strzalka, D. Zheng, F. S. Melkonyan, J. Yan, J. F. Stoddart, S. Fabiano, D. M. DeLongchamp, M. Zhu, A. Facchetti and T. J. Marks, *PNAS*, 2020, **117**, 17551-17557.
58. Y. Nishimuraa, D. Yoshida, M. Mizuhata, K. Asaka, K. Oguro and H. Takenak, *Energy Convers. Manage.*, 1995, **36**, 629-632.
59. X. Zhang, Y. Wang, M. Gu, M. Wang, Z. Zhang, W. Pan, Z. Jiang, H. Zheng, M. Lucero, H. Wang, G. E. Sterbinsky, Q. Ma, Y.-G. Wang, Z. Feng, J. Li, H. Dai and Y. Liang, *Nat. Energy*, 2020, **5**, 684-692.
60. Y. Wang, Y. Li, J. Liu, C. Dong, C. Xiao, L. Cheng, H. Jiang, H. Jiang and C. Li, *Angew. Chem. Int. Ed.*, 2021, **60**, 7681-7685.
61. F. Li, Y. C. Li, Z. Wang, J. Li, D.-H. Nam, Y. Lum, M. Luo, X. Wang, A. Ozden, S.-F. Hung, B. Chen, Y. Wang, J. Wicks, Y. Xu, Y. Li, C. M. Gabardo, C.-T. Dinh, Y. Wang, T.-T. Zhuang, D. Sinton and E. H. Sargent, *Nat. Catal.*, 2019, **3**, 75-82.
62. Z. Chen, T. Wang, B. Liu, D. Cheng, C. Hu, G. Zhang, W. Zhu, H. Wang, Z.-J. Zhao and J. Gong, *J. Am. Chem. Soc.*, 2020, **142**, 6878-6883.
63. W. Ma, S. Xie, T. Liu, Q. Fan, J. Ye, F. Sun, Z. Jiang, Q. Zhang, J. Cheng and Y. Wang, *Nat. Catal.*, 2020, **3**, 478-487.
64. R. Kas, K. K. Hummadi, R. Kortlever, P. de Wit, A. Milbrat, M. W. Luiten-Olieman, N. E. Benes, M. T. M. Koper and G. Mul, *Nat. Commun.*, 2016, **7**, 10748.
65. E. J. Dufek, T. E. Lister and M. E. McIlwain, *J. Appl. Electrochem.*, 2011, **41**, 623-631.
66. R. L. Cook, R. C. MacDuff and A. F. Sammells, *J. Electrochem. Soc.*, 1990, **137**, 607-608.

67. H. Xiang, S. Rasul, B. Hou, J. Portoles, P. Cumpson and E. H. Yu, *ACS Appl. Mater. Interfaces*, 2020, **12**, 601-608.
68. S. Verma, X. Lu, S. Ma, R. I. Masel and P. J. A. Kenis, *Phys. Chem. Chem. Phys.*, 2016, **18**, 7075-7084.
69. Z. Bitar, A. Fecant, E. Trela-Baudot, S. Chardon-Noblat and D. Pasquier, *Appl. Catal. B*, 2016, **189**, 172-180.
70. R. Wang, H. Haspel, A. Pustovarenko, A. Dikhtiarenko, A. Russkikh, G. Shterk, D. Osadchii, S. Ould-Chikh, M. Ma and W. A. Smith, *ACS Energy Lett.*, 2019, **4**, 2024-2031.
71. R. Shi, J. Guo, X. Zhang, G. I. N. Waterhouse, Z. Han, Y. Zhao, L. Shang, C. Zhou, L. Jiang and T. Zhang, *Nat. Commun.*, 2020, **11**, 3028.
72. T. Burdyny and W. A. Smith, *Energy Environ. Sci.*, 2019, **12**, 1442-1453.
73. C.-T. Dinh, T. Burdyny, M. G. Kibria, A. Seifitokaldani, C. M. Gabardo, F. P. G. de Arquer, A. Kiani, J. P. Edwards, P. De Luna, O. S. Bushuyev, C. Zou, R. Quintero-Bermudez, Y. Pang, D. Sinton and E. H. Sargent, *Science*, 2018, **360**, 783-787.
74. Q. Wang, H. Dong, H. Yu and H. Yu, *J. Power Sources*, 2015, **279**, 1-5.
75. K. Junge Puring, D. Siegmund, J. Timm, F. Möllenbruck, S. Schemme, R. Marschall and U. P. Apfel, *Adv. Sustainable Syst.*, 2020, **5**, 2000088.
76. N. Sikdar, J. R. C. Junqueira, S. Dieckhofer, T. Quast, M. Braun, Y. Song, H. B. Aiyappa, S. Seisel, J. Weidner, D. Ohl, C. Andronescu and W. Schuhmann, *Angew. Chem. Int. Ed.*, 2021, DOI: [10.1002/anie.202108313](https://doi.org/10.1002/anie.202108313).
77. L. Jiao, W. Yang, G. Wan, R. Zhang, X. Zheng, H. Zhou, S.-H. Yu and H.-L. Jiang, *Angew. Chem. Int. Ed.*, 2020, **59**, 20589-20595.

78. M. Luo, Z. Wang, Y. C. Li, J. Li, F. Li, Y. Lum, D.-H. Nam, B. Chen, J. Wicks, A. Xu, T. Zhuang, W. R. Leow, X. Wang, C.-T. Dinh, Y. Wang, Y. Wang, D. Sinton and E. H. Sargent, *Nat. Commun.*, 2019, **10**, 5814.
79. D. A. Salvatore, D. M. Weekes, J. He, K. E. Dettelbach, Y. C. Li, T. E. Mallouk and C. P. Berlinguette, *ACS Energy Lett.*, 2018, **3**, 149-154.
80. M. Ramdin, A. R. T. Morrison, M. de Groen, R. van Haperen, R. de Kler, L. J. P. van den Broeke, J. P. M. Trusler, W. de Jong and T. J. H. Vlucht, *Ind. Eng. Chem. Res.*, 2019, **58**, 1834-1847.
81. L. M. Aeshala, R. Uppaluri, A. Verma, *Phys. Chem. Chem. Phys.* 2014, **16**, 17588-17594.
82. C. Delacourt, P. L. Ridgway, J. B. Kerr and J. Newman, *J. Electrochem. Soc.*, 2008, **155**, B42-B49.
83. G. Wang, J. Pan, S. P. Jiang and H. Yang, *J. CO₂ Util.*, 2018, **23**, 152-158.
84. Q. He, D. Liu, J. H. Lee, Y. Liu, Z. Xie, S. Hwang, S. Kattel, L. Song and J. G. Chen, *Angew. Chem. Int. Ed.*, 2020, **59**, 3033-3037.
85. Y. Wang, C. Niu, Y. Zhu, D. He and W. Huang, *ACS Appl. Energy Mater.*, 2020, **3**, 9841-9847.
86. Y. Liu, D. Tian, A. N. Biswas, Z. Xie, S. Hwang, J. H. Lee, H. Meng and J. G. Chen, *Angew. Chem. Int. Ed.*, 2020, **59**, 11345-11348.
87. C.-Y. Wang, *Chem. Rev.*, 2004, **104**, 4727-4765.
88. A. Weber and J. Newman, *Chem. Rev.*, 2004, **104**, 4679-4726.
89. A. Kusoglu and A. Z. Weber, *Chem Rev*, 2017, **117**, 987-1104.

90. A. Collier, H. Wang, X. Yuan, J. Zhang, and D. Wilkinson, *Int. J. Hydrogen Energy*, 2006, **31**, 1838-1854.
91. D. A. Schiraldi, *Polym. Rev.*, 2006, **46**, 315-327.
92. T. Xie and C. Hayden, *Polymer*, 2007, **48**, 5947-5506.
93. A. A. Shah, T. R. Ralph and F. C. Walsh, *J. Electrochem. Soc.*, 2009, **156**, B465-B484.
94. F. Akinori, S. Hironori and T. Takashi, *Computational and Theoretical Chemistry*, 2017, **1121**, 44-48.
95. J. Zhang, W. Luo and A. Züttel, *J Catal*, 2020, **385**, 140-145.
96. R. B. Kutz, Q. Chen, H. Yang, S. D. Sajjad, Z. Liu and I. R. Masel, *Energy Technol.*, 2017, **5**, 929-936.
97. F. P. G. de Arquer, C.-T. Dinh, A. Ozden, J. Wicks, C. McCallum, A. R. Kirmani, D.-H. Nam, C. Gabardo, A. Seifitokaldani, X. Wang, Y. C. Li, F. Li, J. Edwards, L. J. Richter, S. J. Thorpe, D. Sinton and E. H. Sargent, *Science*, 2020, **367**, 661-666.
98. Y. Wang, Z. Wang, C.-T. Dinh, J. Li, A. Ozden, M. Golam Kibria, A. Seifitokaldani, C.-S. Tan, C. M. Gabardo, M. Luo, H. Zhou, F. Li, Y. Lum, C. McCallum, Y. Xu, M. Liu, A. Proppe, A. Johnston, P. Todorovic, T.-T. Zhuang, D. Sinton, S. O. Kelley and E. H. Sargent, *Nat. Catal.*, 2019, **3**, 98-106.
99. C. Chen, X. Yan, S. Liu, Y. Wu, Q. Wan, X. Sun, Q. Zhu, H. Liu, J. Ma, L. Zheng, H. Wu and B. Han, *Angew. Chem. Int. Ed.*, 2020, **59**, 16459-16464.
100. G. O. Larrazábal, P. Strøm-Hansen, J. P. Heli, K. Zeiter, K. T. Therkildsen, I. Chorkendorff and B. Seger, *ACS Appl. Mater. Interfaces*, 2019, **11**, 41281-41288.

101. M. Wang, N. Preston, N. Xu, Y. Wei, Y. Liu and J. Qiao, *ACS Appl. Mater. Interfaces*, 2019, **11**, 6881-6889.
102. S. Z. Oener, M. J. Foster and S. W. Boettcher, *Science*, 2020, **369**, 1099-1103.
103. C. Xie, Y. Liu, W. Lu, H. Zhang and X. Li, *Energy Environ. Sci.*, 2019, **12**, 1834-1839.
104. Z. Wang, J. Parrondo, C. He, S. Sankarasubramanian and V. Ramani, *Nat. Energy*, 2019, **4**, 281-289.
105. M. Manohar and D. Kim, *ACS Sustainable Chem. Eng.*, 2019, **7**, 16493-16500.
106. J. Xu, I. Amorim, Y. Li, J. Li, Z. Yu, B. Zhang, A. Araujo, N. Zhang and L. Liu, *Carbon Energy*, 2020, **2**, 646-655.
107. K. Sun, R. Liu, Y. Chen, E. Verlage, N. S. Lewis and C. Xiang, *Adv. Energy Mater.*, 2016, **6**, 1600379.
108. B. Mayerhöfer, D. McLaughlin, T. Böhm, M. Hegelheimer, D. Seeberger and S. Thiele, *ACS Appl. Energy Mater.*, 2020, **3**, 9635-9644.
109. M. D. Eisaman, L. Alvarado, D. Larner, P. Wang, B. Garg and K. A. Littau, *Energy Environ. Sci.*, 2011, **4**, 1319-1328.
110. W.-H. Cheng, M. H. Richter, I. Sullivan, D. M. Larson, C. Xiang, B. S. Brunshwig and H. A. Atwater, *ACS Energy Lett.*, 2020, **5**, 470-476.
111. Y. C. Li, Z. Yan, J. Hitt, R. Wycisk, P. N. Pintauro and T. E. Mallouk, *Adv. Sustainable Syst.*, 2018, **2**, 1700187.
112. D. A. Vermaas and W. A. Smith, *ACS Energy Lett.*, 2016, **1**, 1143-1148.
113. M. D. Salazar-Villalpando, *ECS Transactions*, 2011, **33**, 77-88.

114. K. Nakata, T. Ozaki, C. Terashima, A. Fujishima and Y. Einaga, *Angew. Chem. Int. Ed.*, 2014, **53**, 871-874.
115. J.-B. Vennekötter, T. Scheuermann, R. Sengpiel and M. Wessling, *J. CO₂ Util.*, 2019, **32**, 202-213.
116. A. S. Varela, M. Kroschel, N. D. Leonard, W. Ju, J. Steinberg, A. Bagger, J. Rossmeisl and P. Strasser, *ACS Energy Lett.*, 2018, **3**, 812-817.
117. B. M. Setterfield-Price and R. A. W. Dryfe, *J. Electroanal. Chem.*, 2014, **730**, 48-58.
118. J. He, A. Huang, N. J. J. Johnson, K. E. Dettelbach, D. M. Weekes, Y. Cao and C. P. Berlinguette, *Inorg. Chem.*, 2018, **57**, 14624-14631.
119. P. K. Jiwanti and Y. Einaga, *Chem Asian J*, 2020, **15**, 910-914.
120. A. Murata and Y. Hori, *Bull. Chem. Soc. Jpn.*, 1991, **64**, 123-127.
121. N. Yoshihara, M. Arita and M. Noda, *Chem. Lett.*, 2017, **46**, 125-127.
122. J. Resasco, L. D. Chen, E. Clark, C. Tsai, C. Hahn, T. F. Jaramillo, K. Chan and A. T. Bell, *J. Am. Chem. Soc.*, 2017, **139**, 11277-11287.
123. E. Pérez-Gallent, G. Marcandalli, M. C. Figueiredo, F. Calle-Vallejo and M. T. M. Koper, *J. Am. Chem. Soc.*, 2017, **139**, 16412-16419.
124. Y. Lum, B. Yue, P. Lobaccaro, A. T. Bell and J. W. Ager, *J. Phys. Chem. C*, 2017, **121**, 14191-14203.
125. M. R. Thorson, K. I. Siil and P. J. A. Kenis, *J. Electrochem. Soc.*, 2013, **160**, F69-F74.
126. M. C. O. Monteiro, F. Dattila, B. Hagedoorn, R. García-Muelas, N. López and M. T. M. Koper, *Nature Catalysis*, 2021, DOI: 10.1038/s41929-021-00655-5.

127. M. R. Singh, Y. Kwon, Y. Lum, J. W. Ager and A. T. Bell, *J. Am. Chem. Soc.*, 2016, **138**, 13006-13012.
128. J. N. Mills, I. T. McCrum and M. J. Janik, *Phys. Chem. Chem. Phys.*, 2014, **16**, 13699-13707.
129. S. Sato, K. Saita, K. Sekizawa, S. Maeda and T. Morikawa, *ACS Catal.*, 2018, **8**, 4452-4458.
130. J. E. Huang, F. Li, A. Ozden, A. Sedighian Rasouli, F. P. García de Arquer, S. Liu, S. Zhang, M. Luo, X. Wang, Y. Lum, Y. Xu, K. Bertens, R. K. Miao, C.-T. Dinh, D. Sinton and E. H. Sargent, *Science*, 2021, **372**, 1074-1078.
131. J. Resasco, Y. Lum, E. Clark, J. Z. Zeledon and A. T. Bell, *ChemElectroChem*, 2018, **5**, 1064-1072.
132. Y. Hori, A. Murata, R. Takahashi and S. Suzuki, *J. Chem. Soc., Chem. Commun.*, 1988, 17-19.
133. C. Chen, Y. Li and P. Yang, *Joule*, 2021, **5**, 737-742.
134. Y. Hori, A. Murata and R. Takahashi, *J. Chem. Soc., Faraday Trans. I*, 1989, **85**, 2309-2326.
135. B. Zhang, J. Zhang, M. Hua, Q. Wan, Z. Su, X. Tan, L. Liu, F. Zhang, G. Chen, D. Tan, X. Cheng, B. Han, L. Zheng and G. Mo, *J. Am. Chem. Soc.*, 2020, **142**, 13606-13613.
136. A. S. Varela, M. Kroschel, T. Reier and P. Strasser, *Catal. Today*, 2016, **260**, 8-13.
137. I. Hitoshi, T. Koji and T. Toshio, *Organometallics*, 1987, **6**, 181-186.
138. Y. Hori, A. Murata, R. Takahashi and S. Suzuki, *J. Am. Chem. Soc.*, 1987, **109**, 5022-5023.

139. Y. Hori, R. Takahashi, Y. Yoshinami and A. Murata, *J. Phys. Chem. B*, 1997, **101**, 7075-7081.
140. S. E. Weitzner, S. A. Akhade, J. B. Varley, B. C. Wood, M. Otani, S. E. Baker and E. B. Duoss, *J. Phys. Chem. Lett.*, 2020, **11**, 4113-4118.
141. X. Lu, C. Zhu, Z. Wu, J. Xuan, J. S. Francisco and H. Wang, *J. Am. Chem. Soc.*, 2020, **142**, 15438-15444.
142. L. Wang, S. A. Nitopi, E. Bertheussen, M. Orazov, C. G. Morales-Guio, X. Liu, D. C. Higgins, K. Chan, J. K. Nørskov, C. Hahn and T. F. Jaramillo, *ACS Catal.* 2018, **8**, 7445-7454.
143. M. Jouny, W. Luc and F. Jiao, *Nat. Catal.*, 2018, **1**, 748-755.
144. H. Mistry, F. Behafarid, R. Reske, A. S. Varela, P. Strasser and B. Roldan Cuenya, *ACS Catal.*, 2016, **6**, 1075-1080.
145. A. S. Varela, W. Ju, T. Reier and P. Strasser, *ACS Catal.*, 2016, **6**, 2136-2144.
146. Y. Huang, C. W. Ong and B. S. Yeo, *ChemSusChem*, 2018, **11**, 3299-3306.
147. D. Gao, F. Scholten and B. Roldan Cuenya, *ACS Catal.*, 2017, **7**, 5112-5120.
148. D. Gao, I. Sinev, F. Scholten, R. M. Arán-Ais, N. J. Divins, K. Kvashnina, J. Timoshenko and B. Roldan Cuenya, *Angew. Chem. Int. Ed.*, 2019, **58**, 17047-17053.
149. Y. Oh, H. Vrabel, S. Guidoux and X. Hu, *Chem. Commun.*, 2014, **50**, 3878-3881.
150. N. E. Mendieta-Reyes, W. Cheuquepán, A. Rodes and R. Gómez, *ACS Catal.*, 2019, **10**, 103-113.
151. C. I. Shaughnessy, D. J. Sconyers, H.-J. Lee, B. Subramaniam, J. D. Blakemore and K. C. Leonard, *Green Chem.*, 2020, **22**, 2434-2442.

152. C. Jiang, A. W. Nichols, J. F. Walzer and C. W. Machan, *Inorg. Chem.*, 2020, **59**, 1883-1892.
153. Y. Tomita, S. Teruya, O. Koga and Y. Hori, *J. Electrochem. Soc.*, 2000, **147**, 4164-4167.
154. A. Aljabour, H. Coskun, D. H. Apaydin, F. Ozel, A. W. Hassel, P. Stadler, N. S. Sariciftci and M. Kus, *Appl. Catal. B*, 2018, **229**, 163-170.
155. J. Shi, F. Shi, N. Song, J.-X. Liu, X.-K. Yang, Y.-J. Jia, Z.-W. Xiao and P. Du, *J. Power Sources*, 2014, **259**, 50-53.
156. Y. Matsubara, D. C. Grills and Y. Kuwahara, *ACS Catal.*, 2015, **5**, 6440-6452.
157. F. Zhang, H. Zhang and Z. Liu, *Curr. Opin. Green Sust.*, 2019, **16**, 77-84.
158. M. M. de Salles Pupo and R. Kortlever, *ChemPhysChem*, 2019, **20**, 2926-2935.
159. D. R. MacFarlane, M. Forsyth, P. C. Howlett, M. Kar, S. Passerini, J. M. Pringle, H. Ohno, M. Watanabe, F. Yan, W. Zheng, S. Zhang and J. Zhang, *Nat. Rev. Mater.*, 2016, **1**, 15005.
160. X. Zhao, S. Li, H. Cheng, J. Schmidt and A. Thomas, *ACS Appl. Mater. Interfaces*, 2018, **10**, 3912-3920.
161. L. E. Barrosse-Antle, C. Hardacre and R. G. Compton, *J. Phys. Chem. B*, 2009, **113**, 2805-2809.
162. B. A. Rosen, A. Salehi-Khojin, M. R. Thorson, W. Zhu, D. T. Whipple, P. J. A. Kenis and R. I. Masel, *Science*, 2011, **334**, 643-644.
163. D.-W. Yang, Q.-Y. Li, F.-X. Shen, Q. Wang, L. Li and N. Song, *Electrochim. Acta*, 2016, **189**, 32-37.
164. H.-K. Lim, Y. Kwon, H. S. Kim, J. Jeon, Y.-H. Kim, J.-A. Lim, B.-S. Kim, J. Choi and H. Kim, *ACS Catal.*, 2018, **8**, 2420-2427.

165. S. Gonell, E. A. Assaf, K. Duffee, C. K. Schauer and A. J. M. Miller, *J. Am. Chem. Soc.*, 2020, **142**, 8980-8999.
166. G.-R. Zhang, S.-D. Straub, L.-L. Shen, Y. Hermans, P. Schmatz, A. M. Reichert, J. P. Hofmann, I. Katsounaros and B. J. M. Etzold, *Angew. Chem. Int. Ed.*, 2020, **59**, 18095-18102.
167. C. Xia, P. Zhu, Q. Jiang, Y. Pan, W. Liang, E. Stavitsk, H. N. Alshareef and H. Wang, *Nat. Energy*, 2019, **4**, 776-785.
168. L. Fan, C. Xia, P. Zhu, Y. Lu and H. Wang, *Nat. Commun.*, 2020, **11**, 3633.



Dui Ma is a postdoctoral researcher jointly trained by Research & Development Institute of Northwestern Polytechnical University in Shenzhen and The Hong Kong Polytechnic University. She received her Ph.D. in 2019 from the Shanghai Jiao Tong University, China. Her research interests include metal-based electrocatalysts for CO₂ reduction and energy devices.



Ting Jin is a professor at the State Key Laboratory of Solidification Processing and the School of Materials Science and Engineering in Northwestern Polytechnic University, China. She received her Ph.D. in 2020 from Nankai University (China) and her B.S. in materials chemistry from Northwest University (China) in 2015. Her research interests focus on design and fabrication of advanced electrode materials for energy storage and conversion, such as rechargeable lithium-ion and sodium-ion batteries.



Keyu Xie is currently a full professor at the Center for Nano Energy Materials, School of Materials Science and Engineering, Northwestern Polytechnical University. His research focuses on energy materials and battery electrochemistry (advanced secondary batteries such as lithiumion batteries, lithium-sulfur batteries, sodiumion batteries, and metal-air batteries).



Haitao Huang is a professor in the Department of Applied Physics, The Hong Kong Polytechnic University. He received his PhD from Nanyang Technological University in 2000. His current research interests include electrochemical energy storage and conversion, and ferroelectric materials for energy applications. He is currently the board committee member of the International Academy of Electrochemical Energy Science (IAOEES).